

# Numerical experiments on vapor diffusion in polar snow and firn and its impact on isotopes using the multi-layer energy balance model Crocus in SURFEX V8.0

Alexandra Touzeau<sup>1</sup>, Amaëlle Landais<sup>1</sup>, Samuel Morin<sup>2</sup>, Laurent Arnaud<sup>3</sup>, Ghislain Picard<sup>3</sup>

<sup>1</sup>LSCE, CNRS UMR8212, UVSQ, Université Paris-Saclay, Gif-sur-Yvette, 91191, France

<sup>2</sup>Météo-France - CNRS, CNRM UMR3589, Centre d'Etudes de la Neige, Grenoble, France

<sup>3</sup>IGE, CNRS UMR5183, Université Grenoble Alpes, Grenoble, France

*Correspondence to:* Alexandra Touzeau (alexandra.touzeau@uib.no)

## Abstract

To evaluate the impact of vapor diffusion onto isotopic composition variations in the snow pits and then in ice cores, we introduced water isotopes in the detailed snowpack model Crocus. At each step and for each snow layer, 1) the initial isotopic composition of vapor is taken at equilibrium with solid phase, 2) a kinetic fractionation is applied during transport, and 3) vapor is condensed or snow is sublimated to compensate deviation to vapor pressure at saturation.

We study the different effects of temperature gradient, compaction, wind compaction and precipitation on the final vertical isotopic profiles. We also run complete simulations of vapor diffusion along isotopic gradients and of vapor diffusion driven by temperature gradients at GRIP, Greenland and at Dome C, Antarctica over periods of 1 or 10 years.

The vapor diffusion tends to smooth the original seasonal signal, with an attenuation of 7 % to 12 % of the original signal over 10 years at GRIP. This is smaller than the observed attenuation in ice cores, indicating that the model attenuation due to diffusion is underestimated or that other processes, such as ventilation, influence attenuation. At Dome C, the attenuation is stronger (18 %), probably because of the lower accumulation and stronger  $\delta^{18}\text{O}$  gradients.

## 1 Introduction

The isotopic ratios of oxygen or deuterium measured in ice cores have been used for a long time to reconstruct the evolution of temperature over the Quaternary (EPICA comm. members, 2004; Johnsen et al., 1995; Jones et al., 2018; Jouzel et al., 2007; Kawamura et al., 2007; Lorius et al., 1985; Petit et al., 1999; Schneider et al., 2006; Stenni et al., 2004; Stenni et al., 2011; Uemura et al., 2012; WAIS-Divide members, 2013). They are however subject to alteration

30 during post-deposition through various processes. Consequently, even if the link between temperature and isotopic  
31 composition of the precipitations is quantitatively determined from measurements and modelling studies (Stenni et al.,  
32 2016; Goursaud et al., 2017), it cannot faithfully be applied to reconstruction of past temperature. Nevertheless, ice  
33 cores remain a primary climatic archive for the Southern Hemisphere where continental archives are rare (Mann and  
34 Jones, 2003). In Antarctica, where meteorological records only started in the 1950s (Genthon et al., 2013), they provide  
35 useful information for understanding climate variability (e.g. EPICA comm. members, 2006; Shaheen et al., 2013;  
36 Steig, 2006; Stenni et al., 2011) and recent climate change (e.g. Altnau et al., 2015; Schneider et al., 2006). When  
37 using ice cores for past climate reconstruction, other parameters than temperature at condensation influence the isotopic  
38 compositions and must be considered. Humidity and temperature in the region of evaporation (Landais et al., 2008;  
39 Masson-Delmotte et al., 2011), or the seasonality of precipitation (Delmotte et al., 2000; Sime et al., 2008; Laepple et  
40 al., 2011) should be taken into account. In addition, uneven accumulation in time and space introduces stratigraphic  
41 noise (Ekaykin et al., 2009). Indeed, records from adjacent snow pits have been shown to be markedly different, under  
42 the influence of decameter-scale local effects such as wind redeposition of snow, erosion, compaction, and  
43 metamorphism (Ekaykin et al., 2014; Petit et al., 1982). These local effects reduce the signal/noise ratio. Then only  
44 stacking a series of records from snow pits can eliminate this local variability and yield information relevant to recent  
45 climate variations (Fisher and Koerner, 1994; Hoshina et al., 2014; Ekaykin et al., 2014; Altnau et al., 2015). This  
46 concern is particularly significant in central regions of east Antarctica characterized by accumulation rates lower than  
47 100 mm water equivalent per year (van de Berg et al., 2006). There, strong winds can scour and erode snow layer over  
48 depths larger than the annual accumulation (Frezzotti et al., 2005; Morse et al., 1999; Libois et al., 2014). There is thus  
49 a strong need to study post-deposition effects in these cold and dry regions.

50 Additionally to mechanical reworking of the snow, the isotopic compositions are further modified in the snowpack.  
51 First, diffusion along isotopic gradients can occur within the snow grains due to solid diffusion (Ramseier et al., 1967).  
52 Second, within the porosity, the vapor isotopic composition can change due to: 1) diffusion along isotopic gradients in  
53 gaseous state, 2) thermally induced vapor transport caused by vapor pressure gradients, 3) ventilation in gaseous state,  
54 or 4) exchanges between the gas phase and the solid phase i.e. sublimation and condensation. In the porosity, the  
55 combination of diffusion along isotopic gradients in the vapor and of exchange between vapor and the solid phase has  
56 been suggested to be the main explanation to the smoothing of the isotopic signal in the solid phase (Ebner et al., 2016,

57 2017; Gkinis et al., 2014; Johnsen et al., 2000). The isotopic compositions in the solid phase is also modified by ‘dry  
58 metamorphism’ and ‘ventilation’ but in a less predictable way. In both cases, the vapor transport exerts an influence  
59 on the isotopic compositions in the solid phase because of permanent exchanges between solid and vapor. During ‘dry  
60 metamorphism’ (Colbeck et al., 1983), vapor transport is driven by vapor pressure gradients, themselves caused by  
61 temperature gradients. During ventilation (Town et al., 2008), vapor moves as part of the air in the porosity, because  
62 of pressure variations at the surface. Last, at the top of the snowpack, the isotopic composition of snow may also be  
63 modified through direct exchange with atmospheric vapor (Ritter et al., 2016).

64 To elucidate the impact of these various post-deposition processes on the snow isotopic compositions, numerical  
65 models are powerful tools. They allow one to discriminate between processes and test their impact one at a time.  
66 Indeed, Johnsen et al. (2000) were able to simulate and deconvolute the influence of diffusion along isotopic gradients  
67 in the vapor at two Greenland ice-core sites, GRIP and NGRIP, using a numerical model. To do this, they define a  
68 quantity named ‘diffusion length’ which is the mean displacement of a water molecule during its residence time in the  
69 porosity. Using a thinning model and an equation of diffusivity of the water isotopes in snow, they compute this  
70 diffusion length as a function of depth. It is then used to compute the attenuation ratio  $A/A_0$ , and in the end retrieve  
71 the original amplitude  $A_0$ . Additionally, the effect of forced ventilation was investigated by Neumann (2003) and  
72 Town et al. (2008) using similar multi-layer numerical models. In these models, wind-driven ventilation forces  
73 atmospheric vapor into snow. There, the vapor is condensed especially in layers colder than the atmosphere.

74 We focus on the movement of water isotopes in the vapor phase in the porosity, in the absence of macroscopic air  
75 movement. In that situation, the movement of vapor molecules in the porosity is caused by vapor pressure gradients,  
76 or by diffusion along isotopic gradients. Note that in the first case, the vapor transport is ‘thermally induced’ i.e. the  
77 vapor pressure gradients directly result from temperature gradients within the snowpack. Thus, the first prerequisite of  
78 our model is to correctly simulate macroscopic energy transfer within the snowpack and energy exchange at the  
79 surface.

80 The transport of vapor molecules will affect the isotopic composition in the solid phase only if exchanges between  
81 vapor and solid are also implemented. Thus, the second prerequisite is that the model includes a description of the  
82 snow microstructure, and of its evolution in time. Snow microstructure is typically represented by its emerging scalar  
83 properties such as density, specific surface area and higher order terms often referred to as “shape parameters” (e.g.

84 Krol and Löwe, 2016). While the concept of “grain” bears ambiguity, it is a widely used term in snow science and  
85 glaciology which we here employ as a surrogate for “elementary microstructure element”, without explicit reference  
86 to a formal definition, be it crystallographic or geometrical.

87 Crocus is a unidimensional multi-layer model of snowpack with a typically centimetric resolution initially dedicated  
88 to the numerical simulation of snow in temperate regions (Brun et al., 1992). It describes the evolution of the snow  
89 microstructure driven by temperature and temperature gradients during dry snow metamorphism, using semi-empirical  
90 variables and laws. It has been used for ice-sheets conditions in polar regions, both Greenland and Antarctica (Brun et  
91 al., 2011; Lefebvre et al., 2003; Fréville et al., 2013; Libois et al., 2014, 2015). In these regions, it gives realistic  
92 predictions of density and snow type profiles (Brun et al., 1992; Vionnet et al., 2012), snow temperature profile (Brun  
93 et al., 2011) and snow specific surface area and permeability (Carmagnola et al., 2014; Domine et al., 2013). It has  
94 been recently optimized for application to conditions prevailing at Dome C, Antarctica (Libois et al., 2014). This was  
95 necessary to account for specific conditions such as high snow density values at the surface and low precipitation  
96 amounts.

97 The Crocus model has high vertical spatial resolution and also includes interactive simulation of snow metamorphism  
98 in near-surface snow and firn. Therefore, it is a good basis for the study of post-deposition effects in low accumulation  
99 regions. For the purpose of this study, we thus implemented vapor transport resulting from temperature gradients and  
100 the water isotopes dynamics into the Crocus model. This article presents this double implementation, and a series of  
101 sensitivity tests. A perfect match of observations is not anticipated, in part because not all relevant processes are  
102 represented in the model. This study represents thus a first step towards better understanding the impact of diffusion  
103 driven by temperature gradients on the snow isotopic composition.

## 104 **2 Physical basis**

105 The isotopic composition of the snow can evolve after deposition due to several processes. Here, we first give a brief  
106 overview of such processes at the macroscopic level. Section 2.1 thus deals with modification of the isotopic  
107 composition of a centimetric/decametric snow layer after exchanges with the other layers. Second, we consider the  
108 evolution of the isotopic composition at the microscopic level, i.e. at the level of the microstructure. Indeed, the  
109 macroscopic change of the isotopic composition results from both large scale and small-scale processes. For instance,

110 dry metamorphism includes both vapor transport from one layer to another, and vapor/ice grain exchange inside a  
111 layer.

## 112 **2.1 Evolution of the snow layers composition at the macroscopic scale**

113 Several studies address the evolution of the isotopic compositions in the snow column after deposition. Here we  
114 describe first processes leading only to attenuation of the original amplitude (Sect. 2.1.1). Then we describe processes  
115 which lead to other types of signal modifications (Sect. 2.1.2). These modifications result from transportation and  
116 accumulation of heavy or light isotopes in some layers without any link to the original isotopic signal. In some cases,  
117 the mean  $\delta^{18}\text{O}$  value of the snow deposited can also be modified.

### 118 **2.1.1 Signal attenuation on a vertical profile: smoothing**

119 In this Section we consider processes leading only to attenuation of the original amplitude of the  $\delta^{18}\text{O}$  signal by  
120 smoothing. We define the mean local pluriannual value as the average isotopic composition in the precipitation taken  
121 over 10 years. The smoothing processes, which act only on signal variability, do not modify this average value. Within  
122 the snow layers, the smoothing of isotopic compositions is caused by diffusion along isotopic gradients in vapor phase  
123 and in solid phase. The magnitude of smoothing depends on site temperature, and on accumulation. Indeed, higher  
124 temperatures correspond to higher vapor concentrations, and higher diffusivities in the vapor and solid phases.  
125 Oppositely, high accumulation rates ensure a greater separation between seasonal  $\delta^{18}\text{O}$  peaks (Ekaykin et al., 2009;  
126 Johnsen et al., 1977) thereby limiting the impact of diffusion. They also result in increased densification rates, and  
127 therefore reduced diffusivities (Gkinis et al., 2014). Because sites with high accumulation rates also usually have higher  
128 temperatures, the resulting effect on diffusion is still unclear. These two competing effects should be thoroughly  
129 investigated and Johnsen et al. (2000) displays the damping amplitude of a periodic signal depending on wavelength  
130 and on diffusion length, strongly driven by temperature.

131 In Greenland, Johnsen et al. (1977) indicate that annual cycles generally disappear at depths shallower than 100 m for  
132 sites with accumulation lower than  $200 \text{ kg m}^{-2} \text{ yr}^{-1}$ . Diffusion along isotopic gradients exists throughout the entire  
133 snow/ice column. It occurs mainly in the vapor phase in the firm, especially in the upper layers with larger porosities.  
134 After pore closure, it takes place mostly in the solid phase, at a much slower rate. Note that in the solid phase, all  
135 isotopes have the same diffusion coefficient.

136 **2.1.2 Signal shift caused by processes leading to oriented vapor transport**

137 We consider here the oriented movement of water molecules forced by external variables such as temperature or  
138 pressure. We use the term ‘oriented’ here to describe an overall movement of water molecules that is different from  
139 their molecular agitation, and externally forced. Three processes can contribute to oriented vapor transport and hence  
140 possible isotopic modification within the snowpack: diffusion, convection, and ventilation (Albert et al., 2002). Brun  
141 et Touvier (1987) have demonstrated that convection of dry air within the snow occurs only in case of very low snow  
142 density of the order of  $\sim 100 \text{ kg/m}^3$ . These conditions are generally not encountered in Antarctic snow and therefore  
143 convection is not considered here. Bartelt et al. (2004) also indicate that energy transfer by advection is negligible  
144 compared to energy transfer by conduction in the first meters of the snowpack. The two other processes, ventilation  
145 and diffusion are forced respectively by variations of the surface pressure and surface temperature. In the first case,  
146 the interaction between wind and surface roughness is responsible for wind-pumping, i.e. renewal of the air of the  
147 porosity through macroscopic air movement (Albert et al., 2002; Colbeck, 1989, Neumann et al., 2004). In the second  
148 case, air temperature diurnal or seasonal variations generate vertical temperature gradients within the snow (Albert and  
149 McGilvary, 1992; Colbeck, 1983). They result into vertical vapor pressure gradients, responsible for vapor diffusion.  
150 These two processes are largely exclusive (Town et al., 2008) because strong ventilation homogenize the air and vapor  
151 in the porosity and therefore prevents diffusion. Diffusion as a result of temperature gradients can coexist with  
152 ventilation only at very low air velocities (Calonne et al., 2015). It becomes the main process of vapor transport when  
153 air is stagnant in the porosity. During diffusion, lighter molecules move more quickly in the porosity, leading to a  
154 kinetic fractionation of the various isotopologues.

155 **2.2 Evolution of the isotopic composition at the microscopic scale**

156 **2.2.1 Conceptual representation of snow microstructure as spherical grains**

157 The term “snow grain” as used classically is an approximation. In reality, ‘snow grains’ are very diverse in size, shape,  
158 degree of metamorphism and may also be made of several snow crystals agglomerated. Moreover, they are often  
159 connected to each other, forming an ice matrix, or ‘snow microstructure’. However, several studies addressing snow  
160 metamorphism physical processes have relied on spherical ice elements to represent snow grains and snow  
161 microstructure (Legagneux and Domine, 2005; Flanner and Zender, 2006). Here, we consider that the snow grains are

162 made of two concentric layers, one internal and one external, with different isotopic compositions. In terms of snow  
 163 microstructure, this could correspond to inner vs. outer regions of the snow microstructure.

164 Indeed, the snow grain or microstructure is not necessarily homogeneous in terms of isotopic composition. On the one  
 165 hand, the central part of the grain or of the microstructure is relatively insulated. This central part becomes even more  
 166 insulated as the grain grows, or as the structure gets coarser. On the other hand, outer layers are not necessarily formed  
 167 at the same time as the central part, or in the same environment (Lu and DePaolo, 2016). They are prone to subsequent  
 168 sublimation or condensation of water molecules, implying that their composition varies more frequently than for the  
 169 inner layers. Of course, only the bulk  $\delta^{18}\text{O}$  value of the snow grain can be measured by mass spectrometry. But  
 170 considering the heterogeneity of the grain may be required to get a fine understanding of the processes. In the following,  
 171 we propose to split the ice grain compartment into two sub-compartments: grain surface and grain center. Thus, the  
 172 grain surface isotopic composition evolves because of exchange with two compartments: 1) with vapor in the porosity  
 173 through sublimation or condensation, and 2) with grain center through solid diffusion, or grain center translation. The  
 174 grain center composition evolves at the time scale of week/month, as opposed to the grain surface, where the  
 175 composition changes at the time scale of the vapor diffusion, i.e. over minutes.

### 176 **2.2.2 Solid diffusion within snow grains**

177 The grain center isotopic composition may change either as a result of crystal growth/sublimation or as a result of  
 178 solid diffusion within the grain. For solid diffusion, water molecules move in the crystal lattice through a vacancy  
 179 mechanism, in a process of self-diffusion that has no particular direction, and that is very slow. The diffusivity of  
 180 water molecules in solid ice  $D_{ice}$  in  $\text{m}^2\cdot\text{s}^{-1}$  follows Arrhenius law. Thus, it can be expressed as a function of ice  
 181 temperature  $T$  (Gkinis et al., 2014; Johnsen et al., 2000; Ramseier, 1967) using Eq. (1):

$$182 \quad D_{ice} = 9.2 \cdot 10^{-4} \times \exp\left(\frac{-7186}{T}\right) \quad (1)$$

183 where symbols are listed in Table 1.

184 Thus at 230 K, the diffusivity is  $2.5 \times 10^{-17} \text{m}^2\cdot\text{s}^{-1}$ . Gay et al. (2002) indicate that in the first meter at Dome C, a typical  
 185 snow grain has a radius of 0.1 mm. Across this typical snow grain, the characteristic time for diffusion is given by Eq.  
 186 (2):

$$187 \quad \Delta t_{sol} = \frac{R_{moy}^2}{D_{ice}} = 4.03 \times 10^8 \text{ s, or } \sim 13 \text{ years} \quad (2)$$

188 Therefore, the solid diffusion within the grain is close to zero at the time scales considered in the model. For Dome C,  
189 if we use the average temperature  $T$  of 248 K for the summer months (Dec. to Jan., Table 2), the characteristic time  
190 becomes 15 months. Thus, within a summer period, the snow grain is only partially refreshed through this process. At  
191 Summit the grain size is typically larger, from 0.2 to 0.25 mm in wind-blown and wind pack and from 0.5 to 2 mm in  
192 the depth hoar layer (Albert and Shultz, 2002). The summer temperature is also higher, with an average value  $T$  of 259  
193 K at Summit from July to Sept, after Shuman et al. (2001). Using a grain size of 0.25 mm, the resulting characteristic  
194 time is of the order of 30 months.

### 195 **2.2.3 Snow grain recrystallization**

196 During snow metamorphism, the number of snow grains tends to decrease with time, while the snow grain size tends  
197 to increase (Colbeck, 1983). Indeed, each grain experiences continuous recycling through sublimation/condensation,  
198 but the small grains are more likely to disappear completely. Then, there is no more nucleus for condensation at the  
199 grain initial position. Oppositely, the bigger grains do not disappear and accumulate the vapor released by the smaller  
200 ones. Concurrently to this change of grain size, the grain shape also tends to evolve. In conditions of maintained/stable  
201 temperature gradient, facets appear at the condensing end of snow grains, while the sublimating end becomes rounded  
202 (Colbeck, 1983). In that case, the center of the grain moves toward the warm air region. This migration causes a renewal  
203 of the grain center, on a proportion that can be estimated from the apparent grain displacement (Pinzer et al., 2012).  
204 Pinzer et al. (2012) use this method to obtain an estimation of vapor fluxes.

205 The asymmetric recrystallization of snow grains implies that the surface layer of the snow grain is eroded at one end  
206 and buried at the other end. Therefore, the composition of the grain center changes more often than if the surface layer  
207 was thickening through condensation or thinning through sublimation homogeneously over the grain surface. This  
208 means that the ‘inner core’ of the grain gets exposed more often. Implementing this process is thus very important to  
209 have a real-time evolution of the snow grain center isotopic composition. Here, we reverse the method of Pinzer et al.  
210 (2012). Therefore, we use the fluxes of isotopes in vapor phase computed by the model to assess the renewal of the  
211 grain center (Sect. 3.1.3.).

212 **3 Material and Methods**

213 **3.1 Description of the model SURFEX/Crocus V8.0**

214 We first present the model structure and second describe the new module of vapor transport (diffusion forced by  
215 temperature gradients). Third, we present the integration of water isotopes in the model.

216 **3.1.1 Model structure**

217 The Crocus model is a one-dimensional detailed snowpack model, consisting of a series of snow layers with variable  
218 and evolving thicknesses. Each layer is characterized by its density, heat content, and by parameters describing snow  
219 microstructure such as sphericity and specific surface area (Vionnet et al., 2012, Carmagnola et al., 2014). In the model,  
220 the profile of temperature evolves with time in response to 1) surface temperature and 2) energy fluxes at the surface  
221 and at the base of the snowpack. To correctly compute energy balance, the model integrates albedo calculation,  
222 deduced from surface microstructure and impurity content (Brun et al., 1992, Vionnet et al., 2012).

223 The successive components of the Crocus model have been described by Vionnet et al. (2012). Here we only list them  
224 to describe those modified to include water stable isotopes and water vapor transfer. Note that the Crocus model has a  
225 typical internal time step of 900 s (15 min), corresponding to the update frequency of layers properties. We only refer  
226 here to processes occurring in dry snow.

227 1) Snow fall: The presence/absence of precipitation at a given time is determined from the atmospheric forcing  
228 inputs. When there is precipitation, a new layer of snow may be formed. Its thickness is deduced from the precipitation  
229 amount.

230 2) Update of snow layering: At each step, the model may split one layer into two or merge two layers together  
231 to get closer to a target vertical profile for optimal calculations. This target profile has high resolution in the first layers  
232 to correctly simulate heat and matter exchanges. The layers that are merged together are the closest in terms of  
233 microstructure variables.

234 3) Metamorphism: The microstructure variables evolution follows empirical laws. These laws describe the  
235 change of grain parameters as a function of temperature, temperature gradient, snow density and liquid water content.

236 4) Snow compaction: Layer thickness decreases, and layer density increases under the burden of the overlying  
237 layers and resulting from metamorphism. In the original module, snow viscosity is parameterized using the layer

238 density and also using information on the presence of hoar or liquid water. However, this parameterization of the  
 239 viscosity was designed for alpine snowpack (Vionnet et al., 2012) and may not be adapted to polar snow packs.  
 240 Moreover, since we are considering only the first 12 m of the snowpack in the present simulations, the compaction in  
 241 the considered layers does not compensate the yearly accumulation, leading to rising snow level with time. To maintain  
 242 a stable surface level in our simulations, we used a simplified compaction scheme, where the compaction rate  $\varepsilon$  is the  
 243 same for all the layers. The compaction rate is obtained by dividing the accumulation rate at the site (see Sect. 3.3) by  
 244 the total mass of the snow column (Eq. 3). It is then applied to all layers to obtain the density change per time step  
 245 using Eq. 4.

$$246 \quad \varepsilon = \frac{dm_{sn}}{dt} / \sum_1^{nmax} (\rho_{sn}(t, n) \times dz(t, n)) \quad (3)$$

$$247 \quad \frac{\rho_{sn}(t+dt, n) - \rho_{sn}(t, n)}{dt} = \varepsilon \times \rho_{sn}(t, n) \quad (4)$$

248 5) Wind drift events: They modify the properties of the snow grains which tend to become more rounded. They  
 249 also increase the density of the first layers through compaction. An option allows snow to be partially sublimated  
 250 during these wind drift events (Vionnet et al., 2012).

251 6) Snow albedo and transmission of solar radiation: In the first 3 cm of snow, snow albedo and absorption  
 252 coefficient are computed from snow microstructure properties and impurity content. The average albedo value in the  
 253 first 3 cm is used to determine the part of incoming solar radiation reflected at the surface. The rest of the radiation  
 254 penetrates into the snowpack. Then, the absorption coefficient is used to describe the rate of decay of the radiation as  
 255 it is progressively absorbed by the layers downward, following an exponential law.

256 7) Latent and sensible surface energy and mass fluxes: The sensible heat flux and the latent heat flux are  
 257 computed using the aerodynamic resistance and the turbulent exchange coefficients.

258 8) Vertical snow temperature profile: It is deduced from the heat diffusion equation, using the snow conductivity,  
 259 as well as the energy balance at the top and at the bottom of the snowpack.

260 9) Snow sublimation and condensation at the surface: The amount of snow sublimated/condensed is deduced  
 261 from the latent heat flux, and the thickness of the first layer is updated. Other properties of the first layer such as density  
 262 and SSA are kept constant.

### 263 3.1.2 Implementation of water transfer

264 The new vapor transport subroutine has been inserted after the compaction (4) and wind drift (5) modules, and before  
 265 the solar radiation module (6). In this section, the term ‘interface’ is used for the horizontal surface of exchange between  
 266 two consecutive layers. The flux of vapor at the interface between two layers is obtained using the Fick’s law of  
 267 diffusion (Eq. (5)):

$$268 \quad F(n + 1 \rightarrow n) = \frac{-2 D_{eff}(t,n \rightarrow n+1)(C_v(t,n) - C_v(t,n+1))}{dz(t,n) + dz(t,n+1)} \quad (5)$$

269 where  $dz(t, n)$  and  $dz(t, n+1)$  are the thicknesses of the two layers considered in meters,  $C_v(t, n)$  and  $C_v(t, n+1)$  are the  
 270 local vapor mass concentrations in the two layers in  $\text{kg m}^{-3}$ , and  $D_{eff}(t, n \rightarrow n + 1)$  in  $\text{m}^2 \text{s}^{-1}$  is the effective diffusivity  
 271 of water vapor in the snow at the interface. The thicknesses are known from the previous steps of the Crocus model,  
 272 but the vapor mass concentrations and the interfacial diffusivities must be computed.

273 The effective diffusivity at the interface is obtained in two steps: first the effective diffusivities ( $D_{eff}(t,n)$  and  $D_{eff}(t,n+1)$ )  
 274 in each layer are calculated (Eq. (6)), second, the interfacial diffusivity ( $D_{eff}(t, n \rightarrow n + 1)$ ) is computed as their  
 275 harmonic mean (Eq. (7)). Effective diffusivity can be expressed as a function of the snow density using the relationship  
 276 proposed by Calonne et al. (2014), for layers with relatively low density. In these circumstances, the compaction occurs  
 277 by ‘boundary sliding’, meaning that the grains slide on each other, but that their shape is not modified. It is therefore  
 278 applicable to our study where density is always below  $600 \text{ kg m}^{-3}$ . The equation of Calonne et al. (2014) is based on  
 279 the numerical analysis of 3D tomographic images of different types of snow. It relates normalized effective diffusivity  
 280  $D_{eff} / D_v$  to the snow density  $\rho_{sn}$  in the layer (Eq. (6)).  $D_v$  is the vapor diffusivity in air and has a value that varies  
 281 depending on the air pressure and air temperature (Eq. (19) in Johnsen et al., 2000).  $\rho_{ice}$  corresponds to the density of  
 282 ice and has a value of  $917 \text{ kg m}^{-3}$ .

$$283 \quad \frac{D_{eff}(t,n)}{D_v} = \frac{3}{2} \left( 1 - \frac{\rho_{sn}(t,n)}{\rho_{ice}} \right) - \frac{1}{2} \quad (6)$$

$$284 \quad D_{eff}(t, n \rightarrow n + 1) = \frac{1}{\frac{1}{D_{eff}(t,n)} + \frac{1}{D_{eff}(t,n+1)}} \quad (7)$$

285 We assume that vapor is in general at saturation in the snow layers (Neumann et al., 2008; Neumann et al., 2009). The  
 286 local mass concentration of vapor  $C_v$  in  $\text{kg m}^{-3}$  in each layer is given by the Clausius-Clapeyron equation (Eq. (8)):

$$287 \quad C_v(t, n) = C_{v0} \exp \left( \frac{L_{sub}}{R_v \rho_{ice}} \left( \frac{1}{T_0} - \frac{1}{T(t,n)} \right) \right) \quad (8)$$

288 where  $C_{v0}$  is the mass concentration of vapor at 273.16 K and is equal to  $2.173 \cdot 10^{-3} \text{ kg m}^{-3}$ ,  $L_{sub}$  is the latent heat of  
289 sublimation and has a value of  $2.6 \cdot 10^9 \text{ J m}^{-3}$ ,  $R_v$  is the vapor constant and has a value of  $462 \text{ J kg}^{-1} \text{ K}^{-1}$ ,  $\rho_{ice}$  is the density  
290 of ice and has a value of  $917 \text{ kg m}^{-3}$ ,  $T_0$  is the temperature of the triple point of water and is equal to 273.16 K and T is  
291 the temperature of the layer.

292 All layers are treated identically, except the first layer at the top and the last layer at the bottom. For the uppermost  
293 layer, the exchange of vapor occurs only at the bottom boundary. Indeed, exchanges with the atmosphere are described  
294 elsewhere in Crocus at step 9 where surface energy balance is realized. For the lowermost layer, only exchanges taking  
295 place at the top boundary are considered, the flux of vapor to/from the underlying medium being set to zero.

296 For each layer, the mass concentration of vapor in air and effective diffusivity are computed within the layer and in the  
297 neighboring layers. Fluxes at the top and bottom of each layer are deduced from Fick's law of diffusion (Eq. (5)). They  
298 are integrated over the subroutine time step, and the new mass of the layer is computed. It is used at the beginning of  
299 the next subroutine step. We use a 1 s time step within the subroutine, smaller than the main routine time step of 900  
300 s. This ensures that vapor fluxes remain small relative to the amount of vapor present in the layers. Note that the  
301 temperature profile, which controls the vapor pressure profile, is not modified within the subroutine. Physically,  
302 temperature values should change as a result of the transfer of sensible heat from one layer to another associated with  
303 vapor transport. They should also evolve due to the loss or gain of heat caused by water sublimation or condensation  
304 (Albert and McGilvary, 1992; Kaempfer et al., 2005). However, vapor transport is only a small component to heat  
305 transfer between layers (Albert and Hardy, 1995; Albert and McGilvary, 1992). In the absence of ventilation, with or  
306 without vapor diffusion, the steady-state profile for temperature varies by less than 2% (Calonne et al., 2014). Thus,  
307 the effect can be neglected at first order.

### 308 3.1.3 Implementation of water isotopes

309 In the model, the isotopic composition of snow in each layer is represented by the triplicate ( $\delta^{18}\text{O}$ , d-excess,  $^{17}\text{O}$ -  
310 excess). Only the results of  $\delta^{18}\text{O}$  are presented and discussed here. For each parameter, two values per layer are  
311 considered independently, corresponding to the 'snow grain center' and the 'snow grain surface', respectively. Water  
312 vapor isotopic composition is deduced at each step from the 'snow grain surface' isotopic composition. It is not stored

313 independently to limit the number of prognostic variables. The isotopic compositions are used at step 1, i.e. for  
314 snowfall, and after step 5, within the new module of vapor transfer.

315 In the snow fall subroutine, a new layer of snow may be added, depending on the weather, at the top of the snowpack.  
316 At this step of the routine, the snow grains being deposited are supposed to be homogenous, i.e. they have the same  
317 composition in the “grain surface” compartment and in the “grain center” compartment. Their composition is deduced  
318 from the air temperature (see Sect. 3.2).

319 Within the vapor transport subroutine, a specific module deals with the isotopic aspects of vapor transport. It modifies  
320 the isotopic compositions in the two snow grain sub-compartments as a result of water vapor transport and  
321 recrystallization of snow crystals. It works with four main steps:

322 1) an initiation step where the vapor isotopic compositions are computed, using equilibrium fractionation, from the  
323 ones in the grain surface sub-compartment,

324 2) a transport step where vapor moves from one layer to another, with a kinetic fractionation associated with diffusion,

325 3) a balance step where the new vapor in the porosity exchanges with the grain surface compartment by  
326 sublimation/condensation. The flux is determined by the difference between actual vapor mass concentration and  
327 expected vapor mass concentration at saturation,

328 and 4) a ‘recrystallization’ step where the grain center and grain surface isotopic compositions are homogenized,  
329 leading to an evolution of grain center isotopic composition.

330 The time step in this module is 1s, the same as the time step of the sub-routine.

331 The initial vapor isotope composition  $R_{vap\ ini}^i$  in a given layer is taken at equilibrium with the ‘grain surface’ isotopic  
332 composition  $R_{surf\ ini}^i$ . Here i denotes heavy isotope, and thus stands for  $^{18}\text{O}$ ,  $^{17}\text{O}$  or D. Equilibrium fractionation is a  
333 hypothesis that is correct in layers where vapor has reached equilibrium with ice grains, physically and chemically.

334 This process is limited by the water vapor - snow mass transfer whose associated speed is of the order of 0.09 m.s<sup>-1</sup>  
335 (Albert and McGilvary, 1992). In our case, we are dealing with centimetric scale layers thickness and recalculate the  
336 isotopic composition every second so that we consider that the speed of the mass transfer is not limiting the equilibrium  
337 situation at the water vapor - snow interface. To compute isotopic ratios for water vapor we use the following Eq. (9)  
338 and (10):

$$339 \quad \begin{cases} R_{vap\ ini}^{18} = \alpha_{sub}^{18} \times R_{surf\ ini}^{18} \\ R_{vap\ ini}^{17} = \alpha_{sub}^{17} \times R_{surf\ ini}^{17} \\ R_{vap\ ini}^{18} + R_{vap\ ini}^{17} + 1 = 1/c_{vap\ ini}^{16} \end{cases} \quad (9)$$

$$340 \quad \begin{cases} R_{vap\ ini}^D = \alpha_{sub}^D \times R_{surf\ ini}^D \\ R_{vap\ ini}^D + 1 = 1/c_{vap\ ini}^{1H} \end{cases} \quad (10)$$

341 The equilibrium fractionation coefficients ( $\alpha_{sub}^i$ ) are obtained using the temperature-based parameterization from  
 342 Ellehoj et al. (2013). Note that we make a slight approximation here, by replacing molar concentrations by mass  
 343 concentrations in our mass balance formulas (see Table 1 for symbol definitions).

344 The initial vapor mass concentration in air  $C_v$  has already been computed in the vapor transport subroutine, and the  
 345 volume of the porosity can be obtained from the snow density  $\rho_{sn}$  and the thickness of the layer  $dz$ . By combining  
 346 both, we obtain Eq. (11) which gives the initial mass of vapor in the layer  $m_{vap\ ini}$ .

$$347 \quad m_{vap\ ini} = C_v \times \left(1 - \frac{\rho_{sn}}{\rho_{ice}}\right) \times dz \quad (11)$$

348 This mass of vapor should be subtracted from the initial grain surface mass because vapor mass is not tracked outside  
 349 of the sub-routine (Fig. 1). The new grain surface isotope composition, after vapor individualization is given by Eq.  
 350 (12):

$$351 \quad c_{surf\ new}^{18} = \frac{m_{surf\ new}^{18}}{m_{surf\ new}} = \frac{m_{surf\ ini}^{18} - m_{vap\ ini} \times c_{vap\ ini}^{18}}{m_{surf\ ini} - m_{vap\ ini}} \quad (12)$$

352 The diffusion of isotopes follows the same scheme as the water vapor diffusion described above in Sect. 3.1.2. and Eq.  
 353 (5). In Eq. (13), the gradient of vapor mass concentrations is replaced by a gradient of concentration of the studied  
 354 isotopologue. The kinetic fractionation during the diffusion is realized with the  $D^i/D$  term where  $i$  stands for  $^{18}\text{O}$  or  $^{17}\text{O}$   
 355 or  $^2\text{H}$  (Barkan and Luz, 2007).

$$356 \quad F^{18}(n+1 \rightarrow n) = \frac{-2 \times D_{eff}(t,n \rightarrow n+1) (C_v(t,n) \times c_{vap\ ini}^{18}(t,n) - C_v(t,n+1) \times c_{vap\ ini}^{18}(t,n+1))}{dz(t,n) + dz(t,n+1)} \times \frac{D^{18}}{D} \quad (13)$$

357 As done for water molecules transport (Sect. 3.1.2.), the flux is set to zero at the top of the first layer and at the bottom  
 358 of the last layer. When the vapor concentration is the same in two adjacent layers, the total flux of vapor is null. But  
 359 diffusion along isotopic gradients still occurs if the isotopic gradients are non-zero (Eq. (13)). Once top and bottom  
 360 fluxes of each layer have been computed, the new masses of the various isotopes in the vapor are deduced, as well as  
 361 the new ratios.

362 After the exchanges between layers, the isotopic composition in the vapor has changed. However, the vapor isotopic  
 363 composition is not a prognostic variable outside of the vapor transport subroutine. To record this change, it must be  
 364 transferred to either the ‘grain surface compartment’ or to the ‘grain center compartment’ before leaving the subroutine.  
 365 First, we consider exchanges of isotopes with the grain surface compartment, which is in direct contact with the vapor.  
 366 Depending on the net mass balance of the layer, two situations must be considered:

367 1) If the mass balance is positive, condensation occurs, so that the transfer of isotopes takes place from the vapor  
 368 toward the grain surface. To evaluate the change in the isotope composition in the grain surface, the mass of vapor  
 369 condensed  $\Delta m_{vap,exc}$  must be computed. It is the difference between the mass of vapor expected at saturation and the  
 370 mass of vapor present in the porosity after vapor transport. Note that temperature does not evolve in this sub-routine.  
 371 Nevertheless, the difference is not exactly equal to the mass of vapor that has entered the layer, because of layer  
 372 porosity change. The excess mass of vapor is given by Eq. (14):

$$373 \Delta m_{vap,exc} = \left[ (\rho_{sn\ new} - \rho_{sn\ ini}) + C_v \times \left[ \left( 1 - \frac{\rho_{sn\ ini}}{\rho_{ice}} \right) - \left( 1 - \frac{\rho_{sn\ new}}{\rho_{ice}} \right) \right] \right] \times dz \quad (14)$$

374 Since the excess of vapor is positive, the next step is the condensation of the excess vapor. The number of excess water  
 375 molecules is determined through comparison with the expected number in the water vapor phase for equilibrium state  
 376 between surface snow and water vapor. Here the condensation of excess vapor occurs without additional fractionation  
 377 because (1) there is a permanent isotopic equilibrium between surface snow and interstitial vapor restored at each first  
 378 step of the sub-routine and (2) kinetic fractionation associated with diffusion is taken into account during diffusion of  
 379 the different isotopic species along the isotopic gradients.

380 2) If the mass balance is negative, the transfer of isotopes takes place from the grain surface toward the vapor  
 381 without fractionation. Ice from the grain surface sub-compartment is sublimated without fractionation to reach the  
 382 expected vapor concentration at saturation. Note that the absence of fractionation at sublimation is a frequent  
 383 hypothesis because water molecules move very slowly in ice lattice (Friedman et al., 1991; Neumann et al., 2005;  
 384 Ramseier, 1967). Consequently, the sublimation removes all the water molecules present at the surface of grains,  
 385 including the heaviest ones before accessing inner levels. In reality, there are evidences for fractionation at sublimation.  
 386 It occurs through kinetic effects associated with sublimation / simultaneous condensation, or during equilibrium  
 387 fractionation at the boundary, especially when invoking the existence of a thin liquid layer at the snow – air interface

388 (Neumann et al., 2008 and references therein; Sokratov and Golubev, 2009; Stichler et al., 2001; Ritter et al., 2016).  
389 The new composition in the vapor results from a mixing between the vapor present and the new vapor recently  
390 produced. The composition in the ‘grain surface’ ice compartment does not change.  
391 The limit between the surface compartment and the grain center compartment is defined by the mass ratio of the grain  
392 surface compartment to the total grain mass i.e.  $\tau = m_{surf} / (m_{center} + m_{surf})$ , (Fig. 1). This mass ratio can be used to  
393 determine the thickness of the ‘grain surface layer’ as a fraction of grain radius, for spherical grains. The surface  
394 compartment must be thin, to be able to react to very small changes in mass when vapor is sublimated or condensed.  
395 Our model has a numerical precision of 6 decimals and is run at a 1 s temporal resolution. Consequently, the isotopic  
396 composition of the surface compartment can change in response to surface fluxes only if its mass is smaller than  $10^6$   
397 times the mass of the water vapor present in the porosity. This constrains the maximum value for  $\tau$ :  $m_{surf} < 10^6 m_{vap}$ , or  
398  $m_{surf} / (m_{center} + m_{surf}) < 10^6 \frac{\Phi \cdot \rho_v \cdot V_{tot}}{\rho_{sn} \cdot V_{tot}}$ , i.e.  $\tau < \frac{\rho_v \cdot \Phi}{\rho_{sn}} \cdot 10^6$ . Considering typical temperatures, snow densities and layer  
399 thicknesses (Table 3) we obtain a maximum value of  $3.3 \cdot 10^{-2}$ . On the other hand, this compartment must be thick  
400 enough to transmit the change in isotopic compositions caused by vapor transport and condensation/sublimation to the  
401 grain center. Again, numerical precision imposes that its mass should be no less than  $10^{-6}$  times the mass of the grain  
402 center compartment, and thus we get an additional constraint:  $\tau > 10^{-6}$ . Here we use a ratio  $\tau = 5 \cdot 10^{-4}$  for the mass of the  
403 grain surface relative to the total mass of the layer (Fig. 1). We have run sensitivity tests with smaller and larger ratios  
404 (Sect. 4.3).  
405 Two types of mixing between grain surface and grain center are implemented in the model. The first one is associated  
406 with crystal growth or shrinkage, because of vapor transfer. Mixing is performed at the end of the vapor transfer  
407 subroutine, after sublimation/condensation has occurred. During the exchange of water between vapor and grain  
408 surface, the excess or default of mass in the water vapor caused by vapor transport has been entirely transferred to the  
409 grain surface sub-compartment. Thus, the mass ratio between the grain surface compartment and the grain center  
410 compartment deviates from the original one. To bring the ratio  $\tau$  back to normal value of  $5 \cdot 10^{-4}$ , mass is transferred  
411 either from the grain surface to the grain center or from the grain center to the grain surface. This happens without  
412 fractionation, i.e. if the transfer occurs from the center to the surface, the composition of the center remains constant.  
413 The second type of mixing implemented is the grain center translation (Pinzer et al., 2012) which favors mixing  
414 between grain center and grain surface in the case of sustained temperature gradient. Pinzer et al. (2012) used the

415 apparent grain displacement to compute vapor fluxes. Here, we reverse this method and use the vapor fluxes computed  
416 from Fick's law to estimate the grain center renewal. We could transfer a small proportion of the surface compartment  
417 to the grain center every second. Instead, we choose to totally mix the snow grain every few days. The interval  $\Delta t_{surf/center}$   
418 between two successive mixings is derived from the vapor flux  $F(n+1 \rightarrow n)$  within the layer using Eq. (15).

$$419 \quad \Delta t_{surf/center} = \frac{m_{sn} \times \tau}{F(n+1 \rightarrow n)} \quad (15)$$

420 The average temperature gradient of  $3 \text{ }^\circ\text{C m}^{-1}$  corresponds to a flux  $F(n+1 \rightarrow n)$  of  $1.3 \cdot 10^{-9} \text{ kg} \cdot \text{m}^{-2} \cdot \text{s}^{-1}$ . The typical mass  
421 for the layer  $m_{sn}$  is 3.3 kg. Based on these values, the dilution of the grain surface compartment into the grain center  
422 should occur every 15 days. Of course, this is only an average, since layers have varying masses, and since the  
423 temperature gradient can be larger or smaller. We will however apply this time constant for all the layers and any  
424 temperature gradient (see sensitivity tests Sect. 4.3), to ensure that the mixing between compartments occurs at the  
425 same time in all layers.

426 In terms of magnitude, this process is probably much more efficient for mixing the solid grain than grain growth or  
427 solid diffusion. It is thus crucial for the modification of the bulk isotopic composition of the snow layer. It makes the  
428 link between microscopic processes and macroscopic results.

#### 429 **3.1.4 Model initialization**

430 For model initialization, an initial snowpack is defined, with a fixed number of snow layers, and for each snow layer  
431 an initial value of thickness, density, temperature and  $\delta^{18}\text{O}$ . Typically, processes of oriented vapor transport such as  
432 thermally induced diffusion and ventilation occur mainly in the first meters of snow. Therefore, the model starts with  
433 an initial snowpack of about 12 m.

434 The choice of the layer thicknesses depends on the annual accumulation. Because the accumulation is much higher at  
435 GRIP than at Dome C (Sect. 3.2., Table 2), the second site is used to define the layer thicknesses. About 10 cm of fresh  
436 snow are deposited every year (Genthon et al., 2016; Landais et al., 2017). This implies that to keep seasonal  
437 information, at least one point every 4 cm is required in the first meter. For the initial profile, we impose maximal  
438 thickness of 2 cm for the layers between 0 and 70 cm depth and 4 cm for the layers between 70 cm and 2 meters depth.  
439 As the simulation runs, merging is allowed but restricted in the first meter to a maximum thickness of 2.5 cm. Below

440 2 meters, the thicknesses are set to 40 cm or even 80 cm. Thus, the diffusion process can only be studied in the first 2  
441 m of the model snowpack. In the very first centimeters of the snowpack, thin millimetric layers are used to  
442 accommodate low precipitation amounts and surface energy balance. The initial density profiles are defined for each  
443 site specifically (see Sect. 3.2). The initial temperature and  $\delta^{18}\text{O}$  profiles in the snowpack depend on the simulation  
444 considered (see Sect. 3.3).

### 445 **3.1.5 Model output**

446 A data file containing the spatio-temporal evolution of prognostic variables such as temperature, density, SSA or  $\delta^{18}\text{O}$   
447 is produced for each simulation. Here, we present the results for each variable as two-dimensional graphs, with time  
448 on the horizontal axis and snow height on the vertical axis. The variations of the considered variable are displayed as  
449 color levels. The white color corresponds to an absence of change of the variable. As indicated above, only the first 12  
450 m of the polar snowpack are included in the model. The bottom of this initial snowpack constitutes the vertical  
451 reference or 'zero' to measure vertical heights  $h$ . The height of the top of the snowpack varies with time due to snow  
452 accumulation and to snow compaction. In the text, we sometimes refer to the layer depth  $z$  instead of its height  $h$ . The  
453 depth can be computed at any time by subtracting the current height of the considered layer from the current height of  
454 the top of the snowpack.

### 455 **3.2 Studied sites: meteorology and snowpack description**

456 In this study we run the model under conditions encountered at Dome C, Antarctica and GRIP, Greenland. We chose  
457 these two sites because they have been well-studied in the recent years through field campaigns and numerical  
458 experiments. In particular for Dome C, a large amount of meteorological and isotopic data is available (Casado et al.,  
459 2016a; Stenni et al., 2016; Touzeau et al., 2016). Typical values of the main climatic parameters for the two studied  
460 sites, GRIP and Dome C, are given in Table 2, as well as typical  $\delta^{18}\text{O}$  range. Dome C has lower accumulation rates of  
461 2.7 cm ice equivalent per year (i.e.  $\text{yr}^{-1}$ ) compared to GRIP rates of 23 cm i.e.  $\text{yr}^{-1}$  (Table 2), making it more susceptible  
462 to be affected by post-deposition processes.

463 In this study, we also compare the results obtained for GRIP to results from two other Greenland sites, namely NGRIP  
464 and NEEM. GRIP is located at the ice-sheet summit, whereas the two other sites are located further north, in lower  
465 elevation areas with higher accumulation rates. In detail, NGRIP is located 316 km to the NNW of GRIP ice-drill site

466 (Dahl-Jensen et al., 1997). GRIP and NGRIP have similar temperatures of -31.6 °C and -31.5 °C but different  
 467 accumulation rates of 23 cm i.e. yr.<sup>-1</sup> and 19.5 cm i.e. yr.<sup>-1</sup> respectively. NEEM ice-core site is located some 365 km to  
 468 the NNW of NGRIP on the same ice-ridge. It has an average temperature of -22 °C and an accumulation rate of 22 cm  
 469 i.e. yr.<sup>-1</sup>.

470 The  $\delta^{18}\text{O}$  value in the precipitation at a given site reflects the entire history of the air mass, including evaporation,  
 471 transport, distillation, and possible changes in trajectory and sources. However, assuming that these processes are more  
 472 or less repeatable from one year to the next, it is possible to empirically relate the  $\delta^{18}\text{O}$  to the local temperature, using  
 473 measurements from collected samples. Here, using data from one-year snowfall sampling at Dome C (Stenni et al.,  
 474 2016; Touzeau et al., 2016), we use the following Eq. (16) to link  $\delta^{18}\text{O}$  in the snowfall to the local temperature  $T_{air}$ , in  
 475 K:

$$476 \quad \delta^{18}\text{O}_{sf} = 0.45 \times (T_{air} - 273.15) - 31.5 \quad (16)$$

477 We do not provide an equivalent expression for GRIP, Greenland, because the simulations run here (see Sect. 3.1.1)  
 478 do not include precipitation.

479 The initial density profile in the snowpack is obtained from fitting density measurements from Greenland and  
 480 Antarctica (Bréant et al., 2017). Over the first 12 m of snow, we obtain the following evolution (Eq. (17) and Eq. (18))  
 481 for GRIP and Dome C respectively:

$$482 \quad \rho_{sn}(t, n) = 17.2 \cdot z(t = 0, n) + 310.3 \quad (\text{N}=22; \text{R}^2=0.95) \quad (17)$$

$$483 \quad \rho_{sn}(t, n) = 12.41 \times z(t = 0, n) + 311.28 \quad (\text{N}=293; \text{R}^2=0.50) \quad (18)$$

### 484 3.3 List of simulations

485 Table 4 presents the model configuration for the 6 simulations considered here.

#### 486 3.3.1 Greenland simulations

487 The first simulation, listed as number 1 in Table 4, is dedicated to the study of diffusion along isotopic gradients. It is  
 488 realized on a Greenland snowpack with an initial sinusoidal profile of  $\delta^{18}\text{O}$  (see Eq. 19) and with a uniform and constant  
 489 vertical temperature profile at 241 K. In addition to comparison to  $\delta^{18}\text{O}$  profiles for GRIP and other Greenland sites,  
 490 the aim of the first simulation is to compare results from Crocus model to the models of Johnsen et al. (2000) and  
 491 Bolzan and Pohjola (2000) run at this site with only diffusion along isotopic profiles. To compare our results to theirs,

492 we consider an isothermal snowpack, without meteorological forcing, and we deactivate modules of surface exchanges  
493 and heat transfer. The initial seasonal sinusoidal profile at GRIP is set using Eq. (19):

$$494 \quad \delta^{18}O(t, n) = -35.5 - 8 \times \sin\left(\frac{2\pi \times z(t, n)}{a \times \rho_{ice} / \rho_{sn}(t, n)}\right) \quad (19)$$

495 where  $z$  is the depth of the layer  $n$ ,  $\rho_{sn}$  is its density,  $\rho_{ice}$  is the density of ice and has a value of  $917 \text{ kg m}^{-3}$ ,  $a$  is the  
496 average accumulation at GRIP and is equal to  $0.23 \text{ m i.e./yr}$  (Dahl-Jensen et al., 1993). The peak to peak amplitude  
497 value of  $16 \text{ ‰}$  is close to the back-diffused amplitude at Summit (Sjolte et al., 2011).

498 The second simulation is run with evolving temperature in the snowpack. The snow temperature is computed by the  
499 model, using meteorological forcing from ERA-Interim (see Table 4). In that case, the transport of isotopes in the vapor  
500 phase results both from diffusion along isotopic gradients and from vapor concentration gradients. The initial snowpack  
501 is the same as in the previous simulation.

502 In the two GRIP simulations, the modules of wind compaction and weight compaction are inactive. Indeed, as weight  
503 compaction is taken to compensate yearly accumulation (Eq. (3) and (4)), applying this compaction without  
504 precipitation would lead to an unrealistic drop in snow level. The wind compaction was absent from the model of  
505 Johnsen et al. (2000) and using this module would make comparisons more difficult.

### 506 **3.3.2 Dome C simulations**

507 In simulations 3 to 6, we take advantage of the high documentation of the Dome C site to disentangle the different  
508 effects on the variations of water isotopic composition. All the simulations at Dome C were performed with an evolving  
509 temperature profile. Temperatures in the snow layers were computed using a modified meteorological forcing from  
510 ERA-Interim (Dee et al., 2011; Libois et al., 2014; see details in Table 4), as well as the modules of energy exchange  
511 and transfer. In this series of simulations, the  $\delta^{18}O$  values thus evolve as a result of diverging and/or alternating vapor  
512 fluxes. The simulations are ordered by increasing complexity. First, in Simulation 3, the modules of homogeneous  
513 compaction and wind drift are deactivated, as well as the module of snowfall. Thus, the impact of vapor transport  
514 forced by temperature gradients on the snow isotopic compositions is clearly visible. Then, in Simulation 4, the module  
515 of compaction and the module of wind drift are activated, to see their impact on the isotopes. We use an accumulation  
516 rate  $dm_{sn}/dt$  for Dome C of  $0.001 \text{ kg m}^{-2}$  per 15 min (see Eq. (3)). Next, in Simulation 5, snowfall is added, to assess  
517 how new layers affect snow  $\delta^{18}O$  values. Lastly, in Simulation 6, the model is run over 10 years at Dome C, to build

518 up a snowpack with realistic ‘sinusoidal’ variation in  $\delta^{18}\text{O}$  values.

## 519 **4 Results**

### 520 **4.1 Greenland**

#### 521 **4.1.1 Results of the Crocus simulations (Simulations 1 and 2)**

522 Figure 2 shows the result of Simulation 1, where only diffusion along isotopic gradients is active, as in Johnsen et al.,  
523 2000. As expected the peak to peak amplitude of  $\delta^{18}\text{O}$  cycles is reduced because of diffusion. Over 10 years, from 2000  
524 to 2009, the amplitude decreases by 1.2 ‰ which corresponds to a 7.3 % variation.

525 Figure 3 shows the result of Simulation 2, i.e. with varying temperature in the snowpack. The attenuation is stronger  
526 than the one observed in the previous simulation. The minima at 11.46 m increases by 1.03 ‰ over ten years, and the  
527 maxima at 11.15 m decreases by 0.84 ‰. Thus, the total attenuation is  $\sim 1.9$  ‰ or 11.7 % for this height range. Below,  
528 the attenuation is smaller, with a total attenuation of only 6 % for heights between 10.54 and 10.85 m. If we compare  
529 attenuation for heights 11.46 and 11.56 m in the 1<sup>st</sup> and 2<sup>nd</sup> simulation, we note that including temperature gradients  
530 leads to an increased attenuation by 50 %.

531 Between 11.46 m and 11.56 m, the  $\delta^{18}\text{O}_{\text{gcenter}}$  values increase over ten years by 1 to 4 ‰. This increase is not caused  
532 only by attenuation of the original sinusoidal signal. Indeed, at  $h=11.60$  m, the values get higher than the initial maxima  
533 which was -36 ‰ at 11.64 m. There is therefore a local accumulation of heavy isotopes in this layer as a result of vapor  
534 transport. This maximum corresponds to a local maximum in temperature and is coherent with departure of  $^{18}\text{O}$ -  
535 depleted water vapor from this layer. Thus, thermally induced vapor transport does not only result into signal  
536 attenuation, but can also shift the  $\delta^{18}\text{O}$  value, regardless of the initial sinusoidal variations.

537 Lastly, in the first 2-3 cm of the snowpack, strong depletion is observed over the period, with a decrease by 2 to 3 ‰  
538 instead of 0.5 ‰ when the temperature gradients were absent (Simulation 1). This depletion probably results from  
539 arrival of  $^{18}\text{O}$ -depleted water vapor from warmer layers below. This shows again the influence of temperature gradients  
540 which were absent from the previous simulation. However, note that in this simulation we neglect precipitation and  
541 exchange of vapor with the atmosphere. Thus, the depletion observed here may not occur in natural settings when these  
542 processes are active.

543 In conclusion, at GRIP, the diffusion of vapor as a result of temperature gradients has a double impact on isotopic

544 compositions. It increases the attenuation in the first 60 cm of snow, because of higher vapor fluxes. And it also creates  
545 local isotopic maxima and minima, in a pattern corresponding to temperature gradients in the snowpack but  
546 disconnected from the original  $\delta^{18}\text{O}$  sinusoidal signal.

#### 547 **4.1.2 Comparison with core data**

548 Here, we evaluate the attenuation of the initial seasonal signal in  $\delta^{18}\text{O}$  over 10 years at 2 Greenland ice-core sites,  
549 NEEM and GRIP. For the first site, we use 4 shallow cores (NEEM2010S2, NEEM2008S3, NEEM2007S3,  
550 NEEM2008S2) published in Steen-Larsen et al., 2011 and in Masson-Delmotte et al., 2015. For the second site, we  
551 use one shallow core (1989-S1), published in White et al., 1997. For the GRIP core, only the first 80 meters are  
552 considered. Therefore, the data presented corresponds to deposition and densification conditions like the modern ones.  
553 For NEEM the values of the four cores are taken together. For NEEM and GRIP, the semi-amplitude is computed along  
554 the core. In the first 10 meters, the maximum value every 30 cm is retained, and deeper in the firm, because of  
555 compaction, the maximum value every 20 cm is retained (see also Supp. Material; Fig. 4). For this study, we have  
556 chosen to estimate attenuation on years with a clearly marked seasonal cycle, a strategy that can be debated but at least  
557 documented. Consequently, from this first series of maxima, a second series of maxima is computed, with a larger  
558 window of 1 meter. The ‘attenuated amplitudes’ at each level is then defined as the ratio between these 1-meter maxima  
559 and the initial 1-meter maxima. Maximum semi-amplitudes every 5 m are also computed and displayed on Figure 4.  
560 The 2.5 m attenuation is slightly higher at GRIP, leading to a remaining amplitude of 86 %, than at NEEM where the  
561 remaining amplitude is 90 % (Fig. 4). The amplitude decreases with depth in parallel for the two cores, with the  
562 amplitude at NEEM staying always higher than at GRIP. For comparison with our model, we estimate attenuation after  
563 10 years, i.e. at a depth of  $\sim 5.8$  m for NEEM and  $\sim 5.65$  m for GRIP. The remaining amplitude is 80 % and 72 % at  
564 GRIP and NEEM respectively. Our Simulation 1 produced 7 % of attenuation only on the same duration, showing that  
565 our model, run on an isothermal snowpack, underestimates the attenuation observed in the data.

#### 566 **4.1.3 Comparison with other models**

567 At 2.5 m at NGRIP, Johnsen et al. (2000) simulate remaining amplitude of 77 % (Fig. 4). For a depth of 5.43 m,  
568 corresponding to an age of 10 years, the simulated remaining amplitude is 57 %. For Bolzan and Pohjola (2000), at  
569 GRIP after 10 years, 70 % of the initial amplitude is still preserved. The slower attenuation for Bolzan and Pohjola

570 (2000) compared to Johnsen et al. (2000) may be due more to the different sites considered than to the different models.  
571 Indeed, GRIP has higher accumulation rates that should limit diffusion. Nevertheless, the attenuation of 30 % simulated  
572 by Bolzan and Pohjola at GRIP is stronger than the attenuation of 7 % simulated in our model. Town et al. (2008, Sect.  
573 [31]) found attenuations of a few tenth of per mil after several years when implementing only diffusion, a result  
574 consistent with ours since we get a decrease by 1.2 ‰ after 10 years.

575 We explore below the reasons for discrepancies between models. The equation for effective diffusivity of vapor in firn  
576 used in our study is different from the ones used by Johnsen et al. (2000) or by Bolzan and Pohjola (2000). Indeed, we  
577 do not consider the tortuosity factor  $l$ , nor the adjustable scale factor  $s$  of Bolzan and Pohjola. However, using the  
578 values given by the previous authors for  $l$  and  $s$  lead to  $D_{eff}$  values ranging from  $6.7 \cdot 10^{-6}$  to  $9.9 \cdot 10^{-6} \text{ m}^2 \text{ s}^{-1}$  for a density  
579 of  $350 \text{ kg m}^{-3}$  and a temperature of 241 K which is coherent with our value of  $8.7 \cdot 10^{-6} \text{ m}^2 \text{ s}^{-1}$ . As indicated by Bolzan  
580 and Pohjola (2000), the choice of one equation or another has little impact here.

581 The most probable difference lie in the way diffusion is taken into account. Johnsen et al. (2000) and Bolzan and  
582 Pohjola (2000) use a single equation of diffusion to predict the evolution of the isotopic composition of the layer. In  
583 our case, we specifically compute the fluxes in the vapor each second and at each depth level and deduce the evolution  
584 of  $\delta^{18}\text{O}$  in the grain center, after sublimation/condensation and recrystallization. Denux (1996) and van der Wel et al.  
585 (2015) indicate that the model developed by Johnsen (1977) and used in Johnsen et al. (2000) overestimates the  
586 attenuation compared to observed values. For Denux (1996), the model of Johnsen (1977) should consider the presence  
587 of ice crusts, and maybe also the temperature gradients in the surface snow, to get closer to the real attenuation at  
588 remote Antarctic sites. Van der Wel et al. (2015) have compared the model results to a spike-layer experiment realized  
589 at Summit. Because an artificial snow layer cannot be representative of natural diffusion, they took care to evaluate  
590 diffusion based only on the natural layers present above and below the artificial layer. van der Wel et al. (2015) propose  
591 three causes to the discrepancy between Johnsen et al.'s model prediction and actual measured attenuation at GRIP.  
592 They blame either ice crusts, or a bad knowledge and parametrization of the tortuosity in the first meters of snow,  
593 and/or a bad description of the isotopic heterogeneity within the ice grain. In our model, the grain heterogeneity is  
594 included. Even if the parameters defining the mixing between the two compartments are not very well constrained (see  
595 Sect. 4.3), the attenuation is indeed smaller compared to the Johnsen's model.

596 **4.2 Dome C (Antarctica)**

597 The aim of the Simulations 3 to 6, run at Dome C, is to isolate diffusion from other effects affecting water isotopic  
598 composition, i.e. wind-drift and compaction.

599 **4.2.1 Simulation 3: without precipitation, without wind drift, and without homogeneous compaction**

600 Figure 5 presents the results of temperature evolution (a and b) and  $\delta^{18}\text{O}$  evolution (c and d) for Simulation 3. The  
601 main changes of  $\delta^{18}\text{O}_{\text{gsurf}}$  and  $\delta^{18}\text{O}_{\text{gcenter}}$  occur in summer (Fig. 5c and 5d). On the one hand, the first 20 cm of snow  
602 tend to become  $^{18}\text{O}$ -enriched by +0.2 ‰ for the grain center compartment. On the other hand, the first centimeter  
603 becomes depleted by 1.0 ‰ for grain center. This pattern is coherent with the temperature profiles for the summer  
604 period (Fig. 5a). Indeed, vapor moves out of the warmest layers and toward colder layers where it condensates. This  
605 causes an increase in  $\delta^{18}\text{O}$  in warm layers and a decrease in colder layers. This pattern is also confirmed by snow  
606 density changes (see Fig. S2).

607 During winter, the temperature generally decreases toward the surface (Fig. 5a). Vapor transport is thus reversed in the  
608 first 20 cm, but this only slightly reduces the dispersion of  $\delta^{18}\text{O}_{\text{gcenter}}$  values. On the first of August, the temperature at  
609 the surface temporarily increases to 235 K. This warm event strongly modifies the temperature profile in the snowpack,  
610 and therefore the pattern of vapor transport. It is associated with an increase of  $\delta^{18}\text{O}$  values at the surface, which is  
611 particularly visible for the  $\delta^{18}\text{O}_{\text{gsurf}}$  values (Fig. 5c).

612 Thus, vapor transport can modify  $\delta^{18}\text{O}$  values in surface snow, even in the absence of precipitation or condensation  
613 from the atmosphere. This mechanism could explain the parallel evolution of surface snow isotopic composition and  
614 temperature described by Steen-Larsen et al. (2014) and Touzeau et al. (2016) between precipitation events.

615 **4.2.2 Simulation 4: without precipitation, with wind drift, and with homogeneous compaction**

616 Compaction and wind drift are not supposed to modify directly the  $\delta^{18}\text{O}$  values. However, the change in densities and  
617 layer thicknesses modifies slightly the temperature profile and the diffusivities. These processes thus could have an  
618 indirect impact on  $\delta^{18}\text{O}$  values. Figure 6 shows  $\delta^{18}\text{O}_{\text{gcenter}}$  changes that are reduced compared to the simulation without  
619 wind drift and compaction. This is coherent with a decrease in the density changes associated with vapor transport in  
620 the case with compaction (see Fig. S5).

621 **4.2.3 Simulation 5: with precipitation, with wind drift, with homogeneous compaction**

622 In Simulation 5, we add precipitation to wind and weight compaction effects. Both snowfall and wind compaction are  
623 responsible for irregular changes, respectively positive and negative, of the height of the snowpack (Fig. 7). In the new  
624 deposited layers, the  $\delta^{18}\text{O}_{\text{gcenter}}$  values reflect the  $\delta^{18}\text{O}$  values in the precipitation. They vary as expected from -40 ‰  
625 on the 31<sup>th</sup> of December to -59 ‰ in July (Fig. 7, Fig. S8). The effect of vapor transport is visible only in ‘old’ layers  
626 which were originally homogeneous in terms of  $\delta^{18}\text{O}$ . These old layers, which were reaching the surface in January,  
627 have been buried below the new layers and are found from 11 cm depth downward in December.

628 **4.2.4 Simulations 6: Ten-years simulation at Dome C**

629 Simulations 6 corresponds to a simulation run over 10 years at Dome C, with variable  $\delta^{18}\text{O}$  in the precipitation. Over  
630 these 10 years, about 1 m of snow is deposited. At the end of the simulation, the vertical profile of  $\delta^{18}\text{O}$  in the new  
631 layers has an average value of -49.7 ‰, and a semi-amplitude of 4.5 ‰ (Fig. 8). Here we take into account all the  
632 maxima and minima at a vertical resolution of 9 cm of fresh snow. Based on the atmospheric temperature variations  
633 only, the isotopic composition in the precipitation should vary around an average value of -53.2 ‰, with a semi-  
634 amplitude of 8.6 ‰. The main reason for this difference is the precipitation amounts: large precipitation events in  
635 winter are associated with relatively high  $\delta^{18}\text{O}$  values. The vertical resolution chosen for the model of 2.5 cm may also  
636 contribute to the decrease of the semi-amplitude. Indeed, light snowfall events do not result in the production of a new  
637 surface layer but are integrated into the old surface layer. As expected, the peak to peak amplitude of  $\delta^{18}\text{O}$  variations  
638 is then further reduced as a result of the two vapor diffusion processes and of associated vapor/solid exchanges. The  
639 effect of vapor transport is relatively small. To help its visualization, we selected four layers and displayed the evolution  
640 of  $\delta^{18}\text{O}$  in these layers over the years (Fig. 8d). The selected layers were deposited during winter 2000, and during  
641 summer seasons 2002, 2004, and 2006.

642 For the layer deposited during winter 2000, there is an increase in  $\delta^{18}\text{O}$  values of about +0.8 ‰ over ten years. The  
643 slope is irregular, with the strongest increases occurring during summers, between November and February, when  
644 vapor transport is maximal. The slope is also stronger when the layer is still close to the surface, probably because of  
645 the stronger temperature gradients in the first centimeters of snow (Fig. 8a). For the layers deposited during the  
646 summers, the evolution of  $\delta^{18}\text{O}$  values is symmetric to the one observed for winter 2000. Over 10 years, i.e. between

647 2000 and 2009, the  $\delta^{18}\text{O}$  amplitude thus decreases by about 1.6 ‰. This corresponds to a decrease of 18 % relative to  
648 the initial amplitude in the snow layers. This is higher than the 7 % attenuation modelled in Greenland for constant  
649 temperature, and to the 11.7 % attenuation observed when including diffusion caused by temperature gradients (Sect.  
650 4.1). However, the comparison between the two sites is not straightforward, because of differences in temperature and  
651 accumulation counteracting each other. On the one hand, at GRIP, the diffusion is forced by low vertical gradients of  
652  $\delta^{18}\text{O}$  of the order of  $0.24 \text{ ‰ cm}^{-1}$ . These are much smaller than the typical  $\delta^{18}\text{O}$  gradients at Dome C which are close  
653 to  $1.10 \text{ ‰ cm}^{-1}$ . On the other hand, the temperature of 241 K at GRIP is higher than the 220 K measured at Dome C,  
654 thus favoring diffusion.

### 655 4.3 Sensitivity tests for duration of recrystallization

656 We have shown above that attenuation of the isotopic signal seems too small at least for the GRIP site. In parallel, the  
657 parameters  $\tau$  and  $\Delta t_{\text{surf/center}}$  of the model associated to grain renewal could only loosely be estimated leading to  
658 uncertainty in the attenuation modeling. In this section, we perform some sensitivity tests to quantify how  $\delta^{18}\text{O}$   
659 attenuation can be increased by exploring the uncertainty range on the renewal of the snow grain. Indeed, the assumed  
660 values for the ratio between grain surface and the total mass of the grain  $\tau$  may have been under or over-estimated. The  
661 same is true for the periodicity of mixing between these two compartments  $\Delta t_{\text{surf/center}}$ .

662 The sensitivity tests are first designed for Greenland sites, run for 6 months, with initial amplitude of the sinusoidal  
663  $\delta^{18}\text{O}$  signal of 16 ‰, and a fixed temperature of 241 K in all the layers (Fig. 9). First, we use a periodicity of mixing  
664  $\Delta t_{\text{surf/center}}$  of 15 days and vary the value for the mass ratio  $\tau$ :  $1 \cdot 10^{-6}$ ,  $5 \cdot 10^{-4}$ ,  $3.3 \cdot 10^{-2}$ . In practice, for  $\Delta t_{\text{surf/center}}=15$  days,  
665 we realize mixing on the second and 16<sup>th</sup> of each month. Second, we use the usual value of  $5 \cdot 10^{-4}$  for  $\tau$  and change the  
666 periodicity of the mixing to 2 days.

667 - In the first case, where  $\tau=1 \cdot 10^{-6}$ , and the mixing occurs every 15 days, the grain surface compartment is very  
668 small. Its original sinusoidal  $\delta^{18}\text{O}$  profile disappears in less than one day due to exchanges with vapor (not shown).  
669 The impact on grain center is then very small with an increase of the first minimum by  $\sim 1.0 \cdot 10^{-4} \text{ ‰}$  over 6 months  
670 (Fig. 9a). In this case, the attenuation due to diffusion is even reduced compared to the results displayed above.

671 - In the second case, where  $\tau=5 \cdot 10^{-4}$ , and the mixing occurs every 15 days, the grain surface compartment is  
672 larger, and the attenuation is slower. Thus, in the grain surface compartment, half of the original amplitude still remains

673 at the end of the simulation (not shown). The impact on the grain center compartment is clearly visible with an increase  
674 of the first minimum by of  $2.2 \cdot 10^{-2} \text{‰}$  after 6 months (Fig. 9b).

675 - In the third case, with  $\tau = 3.3 \cdot 10^{-2}$ , and mixing every 15 days, the attenuation of the sinusoidal signal in the  
676 grain surface compartment is only of 1 % because the grain surface compartment is very large. On opposite, attenuation  
677 in the grain center is quite large, i.e. the first minimum increases by  $4.0 \cdot 10^{-2} \text{‰}$  after 6 months (Fig. 9c).

678 - In the fourth case, with  $\tau = 5 \cdot 10^{-4}$  and mixing every 2 days, the first minimum increases by  $4.1 \cdot 10^{-2} \text{‰}$  after 6  
679 months for the grain center compartment (Fig. 9d). It is similar to the attenuation observed in the third case.

680 The results of these sensitivity tests suggest that the impact of vapor transfer on the grain center isotopic compositions  
681 is maximized when the grain surface compartment is large and/or refreshed often. They also show clearly that using a  
682 small grain surface compartment such as  $\tau = 1 \cdot 10^{-6}$  drastically reduces the impact on the grain center isotopic values.  
683 However, our best estimates for  $\tau$  and  $\Delta t_{\text{surf/center}}$  were not chosen randomly (see Sect. 3.1.3). Moreover, the use of  $\tau = 3.3$   
684  $\cdot 10^{-2}$  or  $\Delta t_{\text{surf/center}} = 2$  days leads to a near doubling of the  $\delta^{18}\text{O}$  attenuation (see above). This is not yet sufficient to explain  
685 the gap between our model output for isothermal simulation and the data. However, if this doubling is applicable to  
686 the case with temperature gradients, the attenuation obtained might reach the one observed in the data at GRIP.

687 At Dome C, sensitivity tests show that we can increase the attenuation by a factor of 3 by reducing the mixing time  
688 from 15 to 2 days (Figure 10b-c). Similarly, if the ratio  $\tau$  is put at  $3.3 \cdot 10^{-2}$  instead of  $5 \cdot 10^{-4}$ , attenuation is more than  
689 doubled over 3 years (Figure 10d-e). Thus, at Dome C, the values of  $\tau$  and  $\Delta t_{\text{surf/center}}$  seem to affect more strongly the  
690 attenuation obtained compared to GRIP. This greater sensitivity at Dome C could result from the influence of  
691 temperature gradients, as well as from steeper  $\delta^{18}\text{O}$  gradients caused by the low accumulation. Indeed, the average  
692 layer thickness of 2 cm in the first meter corresponds to  $\sim 4$  points per year at Dome C, but 35 points per year at GRIP.

#### 693 4.4 Additional missing processes

694 In the previous sections, we have seen that model outputs for GRIP generally lead to smaller attenuation than the one  
695 observed in ice-cores. To improve the model compatibility with data, two kinds of approaches are possible. On the one  
696 hand, it would be useful to realize simulations adapted to on-site experiments such as the one by van der Wel et al.  
697 (2015). This would allow verifying how diffusion can be improved in the model. For instance, previous studies have  
698 suggested that water vapor diffusivity within the snow porosity may be underestimated by a factor of 5 (Colbeck,

699 1983), but this is debated (Calonne et al., 2014). On the other hand, we also believe that other processes should probably  
700 be considered to explain the remaining attenuation. Ventilation is an additional process that has already been  
701 implemented in the snow water isotopic model of Town et al. (2008) and Neumann (2003). Because of strong porosity  
702 and sensitivity to surface wind and relief, ventilation is probably as important as diffusion in the top of the firm, even  
703 if diffusion is expected to be more effective at greater depths. Indeed, for the Dome C simulation (Fig. 8), the slope  
704  $d(\delta^{18}\text{O})/dz$  decreases slowly, indicating that diffusion remains almost as active at 60 centimeters than at 10 centimeters  
705 depth. Neumann (2003) indicates that at Taylor Mouth the diffusion becomes the only process of vapor transport below  
706 2 meters depth. For Dome C, for a temperature gradient of  $3\text{ }^{\circ}\text{C m}^{-1}$ , we compute an average speed due to diffusion of  
707  $3\text{ }10^{-6}\text{ m s}^{-1}$ . This is comparable to air speed due to wind pumping of about  $3\text{ }10^{-6}\text{ m s}^{-1}$  within the top meters of snow  
708 at WAIS (Buizert and Severinghaus, 2016). We conclude that, in as much as these results can be applied to Dome C,  
709 the two processes would have comparable impact at this site in the first meters of snow. The next step for Crocus-iso  
710 development is thus to implement ventilation. Finally, we are also aware that in Antarctic central regions, the wind  
711 reworking of the snow has a strong effect in shaping the isotopic signal. A combination of stratigraphic noise and  
712 diffusion could indeed be responsible for creating isotopic cycles of non-climatic origin in the firm (Laepple et al.,  
713 2017). Wind reworking may also contribute to attenuation, by mixing together several layers deposited during different  
714 seasons.

## 715 **5. Conclusions and perspectives**

716 Water vapor transport and water isotopes have been implemented in the Crocus snow model enabling depicting the  
717 temporal  $\delta^{18}\text{O}$  variations in the top 50 cm of the snow in response to new precipitation, evolution of temperature  
718 gradient in the snow and densification. The main process implemented here to explain post-deposition isotopic  
719 variations is diffusion. We have implemented two types of diffusion in vapor phase: 1) water vapor diffusion along  
720 isotopic gradients, and 2) thermally induced vapor diffusion. The vapor diffusion between layers was realized at the  
721 centimetric scale. The consequences of the two vapor diffusion processes on isotopes in the solid phase were  
722 investigated. The solid phase was modelled as snow grains divided in two sub-compartments: (1) a grain surface sub-  
723 compartment in equilibrium with interstitial water vapor and (2) an inner grain only exchanging slowly with the surface  
724 compartment. We parameterized the speed of diffusion through the renewal time of a snow grain and proportion of the

725 two snow grain compartments.

726 Our approach based on a detailed snow model makes it possible to investigate at fine scale various processes explaining  
727 the variations of density and  $\delta^{18}\text{O}$  in the firm. We look specifically at the effect of evolution of the temperature gradient,  
728 new snow accumulation and compaction event linked to wind drift. Over the first 30 cm, the snow density variations  
729 are mainly driven by compaction events linked to wind drift. Vapor transport and long-term compaction have secondary  
730 effects. Below 30 cm, wind drift driven compaction is no more visible. Because of strong temperature gradient and  
731 low density, water vapor transport will have a significant effect down to 60 cm.  $\delta^{18}\text{O}$  is primary driven by variations  
732 in  $\delta^{18}\text{O}$  of precipitation as expected. The seasonal variations are then attenuated by water vapor transport and diffusion  
733 along isotopic gradients, with an increase of these effects at higher temperatures i.e. during summer periods.

734 From 10 years simulations of the Crocus-iso model both at GRIP Greenland and Dome C Antarctica, we have estimated  
735 the post-deposition attenuation of the annual  $\delta^{18}\text{O}$  signal in the snow to about 7-18 % through diffusion. This  
736 attenuation is smaller than the one obtained from isotopic data on shallow cores in Greenland suggesting missing  
737 processes in the Crocus model when implementing water vapor. It is also significantly smaller than the diffusion  
738 implemented by Johnsen et al. (2000) but some studies have suggested that the Johnsen isotopic diffusivity is too  
739 strong (Denux, 1996 ; Van der Wel et al., 2015).

740 We see our study as a first step toward a complete post-deposition modelling of water isotopes variations. Indeed,  
741 several other developments are foreseen in this model. First, wind pumping is currently not implemented in the Crocus  
742 model. This effect, implemented in the approach of Neumann (2003) and Town et al. (2008) is expected to have a  
743 contribution as large as the effect of diffusion for the post-deposition isotopic variations. Second, in low accumulation  
744 sites like Dome C, wind scouring has probably an important effect on the evolution of the  $\delta^{18}\text{O}$  signal in depth through  
745 a reworking of the top snow layers (Libois et al., 2014). This effect has not been considered here but could be  
746 implemented in the model in the next years. It could also play a role in the preservation of anomalously strong  $\delta^{18}\text{O}$   
747 peaks at Dome C (Denux, 1996).

748 Other short-term developments concern the implementation of the exchange of water vapor with the atmosphere  
749 through hoar deposition. This is particularly timely since many recent studies have studied the parallel evolution of  
750 isotopic composition of water vapor and surface snow during summer both in Greenland and Antarctica (Steen-Larsen

751 et al., 2014; Ritter et al., 2016; Casado et al., 2016a; 2016b). Similarly, implementation of ventilation of the snowpack  
752 in the model since this effect is expected to significantly participate to signal attenuation.

753 Another aspect is to look at the post-deposition d-excess and  $^{17}\text{O}$ -excess variations in snow pits. Indeed, recent studies  
754 have shown that the relationship between  $^{17}\text{O}$ -excess and  $\delta^{18}\text{O}$  is not the same when looking at precipitation samples  
755 and snow pits samples in East Antarctica (Touzeau et al, 2016). This observation questions the influence of diffusion  
756 within the snowpack on second order parameters such as  $^{17}\text{O}$ -excess. Indeed,  $^{17}\text{O}$ -excess is strongly influenced by  
757 kinetic diffusion driven fractionation which may be quantified by the implementation of  $^{17}\text{O}$ -excess in our Crocus-iso  
758 model.

759

#### 760 **Code availability**

761 The code used in the manuscript is a development of the open source code for SURFEX/ISBA-Crocus model based  
762 on version V8.0, hosted on an open git repository at CNRM ([https://opensource.umr-cnrm.fr/projects/surfex\\_git2](https://opensource.umr-cnrm.fr/projects/surfex_git2)).  
763 Before downloading the code, you must register as a user at <https://opensource.umr-cnrm.fr/>. You can then obtain  
764 the code used in the present study by downloading the revision tagged 'Touzeau\_jan2018' of the branch touzeau\_dev  
765 (last access: January 2018). The meteorological forcing required to perform the runs is available as a supplement.

766

#### 767 **Author contribution**

768 S. Morin wrote the new module of vapor diffusion. A. Touzeau inserted isotopes and isotope transport into the  
769 numerical code with help of S. Morin for numerical issues and physics and help from A. Landais for concepts and  
770 hypotheses of the theory of isotopes. G. Picard and L. Arnaud provided information and references on snow  
771 microstructure and microphysics as well as direct field experience on site meteorology and accumulation conditions.  
772 A. Touzeau run the simulations and interpreted the results. A. Touzeau and A. Landais wrote the manuscript. All the  
773 authors corrected the manuscript.

774

#### 775 **Competing interests**

776 The authors declare that they have no conflict of interest.

777

778 **Acknowledgements**

779 The research leading to these results has received funding from the European Research Council under the European  
780 Union's Seventh Framework Programme (FP7/2007-30 2013)/ERC grant agreement no. 306045. We want to  
781 acknowledge A. Orsi and M. Casado from LSCE, who contributed to this work through fertile discussions of the model  
782 contents and its applications. We are grateful to M. Casado and C. Bréant for providing snow pit temperature and  
783 density profiles as well as firn density profiles for model initialization. We would like to thank D. Roche for his advice  
784 during model development, as well as on how to make the code available. We are also indebted to J.-Y. Peterschmidt,  
785 who provided continual help and useful tutorials on Fortran and Python languages. We thank M. Lafaysse and V.  
786 Vionnet at CNRM/CEN for help with the model and meteorological driving data. CNRM/CEN and IGE are part of  
787 LabEX OSUG@2020. We thank three anonymous reviewers for their questions and comments, which helped to  
788 improve the present article.

789

790 **References**

- 791 Albert, M. R. and Hardy, J. P.: Ventilation experiments in seasonal snow cover, IAHS Publications-Series of  
792 Proceedings and Reports-Intern Assoc Hydrological Sciences, 228, 41-50, 1995.
- 793 Albert, M. R. and McGilvary, W. R.: Thermal effects due to air flow and vapor transport in dry snow, Journal of  
794 Glaciology, 38, 273-281, 1992.
- 795 Albert, M. R. and Shultz, E. F.: Snow and firn properties and air-snow transport processes at Summit, Greenland,  
796 Atmospheric Environment, 36, 2789-2797, 2002.
- 797 Albert, M. R., Grannas, A. M., Bottenheim, J., Shepson, P. B., and Perron, F. E.: Processes and properties of snow-air  
798 transfer in the high Arctic with application to interstitial ozone at Alert, Canada, Atmospheric Environment, 36, 2779-  
799 2787, 2002.
- 800 Altnau, S., Schlosser, E., Isaksson, E., and Divine, D.: Climatic signals from 76 shallow firn cores in Dronning Maud  
801 land, East Antarctica, The Cryosphere, 9, 925-944, 2015.
- 802 Barkan, E. and Luz, B.: Diffusivity fractionations of  $\text{H}_2^{16}\text{O}/\text{H}_2^{17}\text{O}$  and  $\text{H}_2^{16}\text{O}/\text{H}_2^{18}\text{O}$  in air and their implications for  
803 isotope hydrology, Rapid Communications in Mass Spectrometry, 21, 2999-3005, 2007.
- 804 Bartelt, P., Buser, O., and Sokratov, S. A.: A nonequilibrium treatment of heat and mass transfer in alpine snowcovers,

805 Cold Regions Science and Technology, 39, 219-242, 2004.

806 Bolzan, J. F. and Pohjola, V. A.: Reconstruction of the undiffused seasonal oxygen isotope signal in central Greenland  
807 ice cores, *Journal of Geophysical Research: Oceans*, 105, 22095-22106, 2000.

808 Bréant, C., Martinerie, P., Orsi, A., Arnaud, L., and Landais, A.: Modelling firn thickness evolution during the last  
809 deglaciation: constraints on sensitivity to temperature and impurities, *Clim. Past*, 13, 833-853, 2017.

810 Brun, E. and Touvier, F.: Etude expérimentale de la convection thermique dans la neige, *Le Journal de Physique*  
811 *Colloques*, 48, C1-257-C1-262, 1987.

812 Brun, E., David, P., Sudul, M., and Brunot, G.: A numerical model to simulate snow-cover stratigraphy for operational  
813 avalanche forecasting, *Journal of Glaciology*, 38, 13-22, 1992.

814 Brun, E., Six, D., Picard, G., Vionnet, V., Arnaud, L., Bazile, E., Boone, A., Bouchard, A., Genthon, C., and Guidard,  
815 V.: Snow/atmosphere coupled simulation at Dome C, Antarctica, *Journal of Glaciology*, 57, 721-736, 2011.

816 Buizert, C. and Severinghaus, J. P.: Dispersion in deep polar firn driven by synoptic-scale surface pressure variability,  
817 *The Cryosphere*, 10, 2099-2111, 2016.

818 Calonne, N., Geindreau, C., and Flin, F.: Macroscopic modeling for heat and water vapor transfer in dry snow by  
819 homogenization, *The Journal of Physical Chemistry B*, 118, 13393-13403, 2014.

820 Calonne, N., Geindreau, C., and Flin, F.: Macroscopic modeling of heat and water vapor transfer with phase change in  
821 dry snow based on an upscaling method: Influence of air convection, *Journal of Geophysical Research: Earth Surface*,  
822 120, 2476-2497, 2015.

823 Carmagnola, C. M., Morin, S., Lafaysse, M., Domine, F., Lesaffre, B., Lejeune, Y., Picard, G., and Arnaud, L.:  
824 Implementation and evaluation of prognostic representations of the optical diameter of snow in the SURFEX/ISBA-  
825 Crocus detailed snowpack model, *The Cryosphere*, 8, 417-437, 2014.

826 Casado, M., Landais, A., Masson-Delmotte, V., Genthon, C., Kerstel, E., Kassi, S., Arnaud, L., Picard, G., Prié, F.,  
827 Cattani, O., Steen-Larsen, H. C., Vignon, E., and Cermak, P.: Continuous measurements of isotopic composition of  
828 water vapour on the East Antarctic Plateau, *Atmos. Chem. Phys. Discuss.*, 16, 8521-8538, 2016a.

829 Casado, M., Landais, A., Picard, G., Münch, T., Laepple, T., Stenni, B., Dreossi, G., Ekaykin, A., Arnaud, L., Genthon,  
830 C., Touzeau, A., Masson-Delmotte, V., and Jouzel, J.: Archival of the water stable isotope signal in East Antarctic ice  
831 cores, *The Cryosphere Discussions*, doi:10.5194/tc-2016-263, 2016b.

832 Colbeck, S. C.: Theory of metamorphism of dry snow, *Journal of Geophysical Research*, 88, 5475-5482, 1983.

833 Colbeck, S. C.: Air movement in snow due to wind pumping, *Journal of Glaciology*, 35, 209-213, 1989.

834 Dahl-Jensen, D., Johnsen, S., Hammer, C., Clausen, H., and Jouzel, J.: Past accumulation rates derived from observed  
835 annual layers in the GRIP ice core from Summit, Central Greenland. In: *Ice in the climate system*, Springer, 1993.

836 Dahl-Jensen, D., Gundestrup, N. S., Keller, K., Johnsen, S. J., Gogineni, S. P., Allen, C. T., Chuah, T. S., Miller, H.,  
837 Kipstuhl, S., and Waddington, E. D.: A search in north Greenland for a new ice-core drill site, *Journal of glaciology*,  
838 43, 300-306, 1997.

839 Dee, D. P., Uppala, S. M., Simmons, A. J., Berrisford, P., Poli, P., Kobayashi, S., Andrae, U., Balmaseda, M. A.,  
840 Balsamo, G., Bauer, P., Bechtold, P., Beljaars, A. C. M., van de Berg, L., Bidlot, J., Bormann, N., Delsol, C., Dragani,  
841 R., Fuentes, M., Geer, A. J., Haimberger, L., Healy, S. B., Hersbach, H., Hólm, E. V., Isaksen, L., Kållberg, P., Köhler,  
842 M., Matricardi, M., McNally, A. P., Monge-Sanz, B. M., Morcrette, J. J., Park, B. K., Peubey, C., de Rosnay, P.,  
843 Tavolato, C., Thépaut, J. N., and Vitart, F.: The ERA-Interim reanalysis: configuration and performance of the data  
844 assimilation system, *Quarterly Journal of the Royal Meteorological Society*, 137, 553-597, 2011.

845 Delmotte, M., Masson, V., Jouzel, J., and Morgan, V. I.: A seasonal deuterium excess signal at Law Dome, coastal  
846 eastern Antarctica: A Southern Ocean signature, *Journal of Geophysical Research: Atmospheres*, 105, 7187-7197,  
847 2000.

848 Denux, F.: Diffusion du signal isotopique dans le névé et dans la glace. Implication pour l'échantillonnage., PhD,  
849 Geosciences, Université Joseph Fourier-Grenoble 1, Grenoble, 243 pp., 1996.

850 Domine, F., Morin, S., Brun, E., Lafaysse, M., and Carmagnola, C. M.: Seasonal evolution of snow permeability under  
851 equi-temperature and temperature-gradient conditions, *The Cryosphere*, 7, 1915-1929, 2013.

852 Ebner, P. P., Schneebeli, M., and Steinfeld, A.: Metamorphism during temperature gradient with undersaturated  
853 advective airflow in a snow sample, *The Cryosphere*, 10, 791-797, 2016.

854 Ebner, P. P., Steen-Larsen, H. C., Stenni, B., Schneebeli, M., and Steinfeld, A.: Experimental observation of transient  
855  $\delta^{18}\text{O}$  interaction between snow and advective airflow under various temperature gradient conditions, *The Cryosphere*,  
856 11, 1733-1743, 2017.

857 Ekaykin, A., Hondoh, T., Lipenkov, V. Y., and Miyamoto, A.: Post-depositional changes in snow isotope content:  
858 preliminary results of laboratory experiments, *Climate of the Past Discussions*, 5, 2239-2267, 2009.

859 Ekaykin, A. A., Kozachek, A. V., Lipenkov, V. Y., and Shibaev, Y. A.: Multiple climate shifts in the Southern  
860 hemisphere over the past three centuries based on central Antarctic snow pits and core studies, *Annals of Glaciology*,  
861 55, 259-266, 2014.

862 Ellehoj, M. D., Steen-Larsen, H. C., Johnsen, S. J., and Madsen, M. B.: Ice-vapor equilibrium fractionation factor of  
863 hydrogen and oxygen isotopes: Experimental investigations and implications for stable water isotope studies, *Rapid*  
864 *Communications in Mass Spectrometry*, 27, 2149-2158, 2013.

865 EPICA comm. members: Eight glacial cycles from an Antarctic ice core, *Nature*, 429, 623-628, 2004.

866 EPICA comm. members: One-to-one coupling of glacial climate variability in Greenland and Antarctica, *Nature*, 444,  
867 195-198, 2006.

868 Fisher, D. A. and Koerner, R. M.: Signal and noise in four ice-core records from the Agassiz Ice Cap, Ellesmere Island,  
869 Canada: details of the last millennium for stable isotopes, melt and solid conductivity, *The Holocene*, 4, 113-120, 1994.

870 Flanner, M. G. and Zender, C. S.: Linking snowpack microphysics and albedo evolution, *Journal of Geophysical*  
871 *Research: Atmospheres*, 111, D12208, doi:10.1029/2005JD006834, 2006.

872 Fréville, H., Brun, E., Picard, G., Tatarinova, N., Arnaud, L., Lanconelli, C., Reijmer, C., and van den Broeke, M.:  
873 Using MODIS land surface temperatures and the Crocus snow model to understand the warm bias of ERA-Interim  
874 reanalyses at the surface in Antarctica, *The Cryosphere*, 8, 1361-1373, 2014.

875 Frezzotti, M., Pourchet, M., Flora, O., Gandolfi, S., Gay, M., Urbini, S., Vincent, C., Becagli, S., Gragnani, R., and  
876 Proposito, M.: Spatial and temporal variability of snow accumulation in East Antarctica from traverse data, *Journal of*  
877 *Glaciology*, 51, 113-124, 2005.

878 Friedman, I., Benson, C., and Gleason, J.: Isotopic changes during snow metamorphism, *Stable isotope geochemistry:*  
879 *a tribute to Samuel Epstein*, 1991. 211-221, 1991.

880 Gay, M., Fily, M., Genthon, C., Frezzotti, M., Oerter, H., and Winther, J.-G.: Snow grain-size measurements in  
881 Antarctica, *Journal of Glaciology*, 48, 527-535, 2002.

882 Genthon, C., Six, D., Gallée, H., Grigioni, P., and Pellegrini, A.: Two years of atmospheric boundary layer observations  
883 on a 45-m tower at Dome C on the Antarctic plateau, *Journal of Geophysical Research: Atmospheres*, 118, 3218-3232,  
884 2013.

885 Genthon, C., Six, D., Scarchilli, C., Ciardini, V., and Frezzotti, M.: Meteorological and snow accumulation gradients

886 across Dome C, East Antarctic plateau, *International Journal of Climatology*, 36, 455-466, 2016.

887 Gkinis, V., Simonsen, S. B., Buchardt, S. L., White, J. W. C., and Vinther, B. M.: Water isotope diffusion rates from  
888 the NorthGRIP ice core for the last 16,000 years – Glaciological and paleoclimatic implications, *Earth and Planetary  
889 Science Letters*, 405, 132-141, 2014.

890 Goursaud, S., Masson-Delmotte, V., Favier, V., Preunkert, S., Fily, M., Gallée, H., Jourdain, B., Legrand, M., Magand,  
891 O., Minster, B., Werner, M.: A 60-year ice-core record of regional climate from Adélie land, coastal Antarctica, *The  
892 Cryosphere*, 11, 343-362, 2017.

893 Hoshina, Y., Fujita, K., Nakazawa, F., Iizuka, Y., Miyake, T., Hirabayashi, M., Kuramoto, T., Fujita, S., and  
894 Motoyama, H.: Effect of accumulation rate on water stable isotopes of near-surface snow in inland Antarctica, *Journal  
895 of Geophysical Research*, 119, 274-283, 2014.

896 Johnsen, S.: Stable isotope homogenization of polar firn and ice, *Isotopes and impurities in snow and ice*, 1, 210-219,  
897 1977.

898 Johnsen, S. J., Dahl-Jensen, D., Dansgaard, W., and Gundestrup, N.: Greenland palaeotemperatures derived from GRIP  
899 bore hole temperature and ice core profiles, *Tellus*, 47B, 624-629, 1995.

900 Johnsen, S. J., Clausen, H. B., Cuffey, K. M., Hoffmann, G., Schwander, J., and Creyts, T.: Diffusion of stable isotopes  
901 in polar firn and ice: the isotope effect in firn diffusion, *Physics of ice core records*, 159, 121-140, 2000.

902 Jones, T. R., Roberts, W. H. G., Steig, E. J., Cuffey, K. M., Markle, B. R., White, J. W. C.: Southern Hemisphere  
903 climate variability forced by Northern Hemisphere ice-sheet topography, *Nature*, 554, doi:10.1038/nature24669, 2018.

904 Jouzel, J., Masson-Delmotte, V., Cattani, O., Dreyfus, G., Falourd, S., Hoffmann, G., Minster, B., Nouet, J., Barnola,  
905 J. M., Chappellaz, J., Fischer, H., Gallet, J. C., Johnsen, S., Leuenberger, M., Loulergue, L., Luethi, D., Oerter, H.,  
906 Parrenin, F., Raisbeck, G., Raynaud, D., Schilt, A., Schwander, J., Selmo, E., Souchez, R., Spahni, R., Stauffer, B.,  
907 Steffensen, J. P., Stenni, B., Stocker, T. F., Tison, J. L., Werner, M., and Wolff, E. W.: Orbital and millennial Antarctic  
908 climate variability over the past 800,000 years, *Science*, 317, 793-796, 2007.

909 Kaempfer, T. U., Schneebeli, M., and Sokratov, S. A.: A microstructural approach to model heat transfer in snow,  
910 *Geophysical Research Letters*, 32, L21503, doi:10.1029/2005GL023873, 2005.

911 Kawamura, K., Parrenin, F., Lisiecki, L., Uemura, R., Vimeux, F., Severinghaus, J. P., Hutterli, M. A., Nakazawa, T.,  
912 Aoki, S., Jouzel, J., Raymo, M. E., Matsumoto, K., Nakata, H., Motoyama, H., Fujita, S., Goto-Azuma, K., Fujii, Y.,

913 and Watanabe, O.: Northern Hemisphere forcing of climatic cycles in Antarctica over the past 360,000 years, *Nature*,  
914 448, 912-916, 2007.

915 Krol, Q., and Löwe, H.: Relating optical and microwave grain metrics of snow: the relevance of grain shape, *The*  
916 *Cryosphere*, 10, 2847-2863, 2016.

917 Laepple, T., Werner, M., and Lohmann, G.: Synchronicity of Antarctic temperatures and local solar insolation on  
918 orbital timescales, *Nature*, 471, 91, 2011.

919 Landais, A., Barkan, E., and Luz, B.: Record of  $\delta^{18}\text{O}$  and  $^{17}\text{O}$ -excess in ice from Vostok Antarctica during the last  
920 150,000 years, *Geophysical Research Letters*, 35, L02709, 2008.

921 Landais, A., Casado, C., Prié, F., Magand, O., Arnaud, L., Ekaykin, A., Petit, J.-R., Picard, G., Fily, M., Minster, B.,  
922 Touzeau, A., Goursaud, S., Masson-Dlemotte, V., Jouzel, J., and Orsi, A.: Surface studies of water isotopes in  
923 Antarctica for quantitative interpretation of deep ice core data, *Comptes Rendus Géosciences*, 349, 139-150, 2017.

924 Legagneux, L., and Domine, F.: A mean field model of the decrease of the specific surface area of dry snow during  
925 isothermal metamorphism, *Journal of Geophysical Research*, 110, doi:10.1029/2004JF000181, 2005.

926 Lefebvre, F., Gallée, H., van Ypersele, J.-P., and Greuell, W.: Modeling of snow and ice melt at ETH Camp (West  
927 Greenland): A study of surface albedo, *Journal of Geophysical Research: Atmospheres*, 108, D8-4231,  
928 doi:10.1029/2001JD001160, 2003.

929 Libois, Q., Picard, G., Arnaud, L., Morin, S., and Brun, E.: Modeling the impact of snow drift on the decameter-scale  
930 variability of snow properties on the Antarctic Plateau, *Journal of Geophysical Research: Atmospheres*, 119, 11662-  
931 11681, 2014.

932 Libois, Q., Picard, G., Arnaud, L., Dumont, M., Lafaysse, M., Morin, S., and Lefebvre, E.: Summertime evolution of  
933 snow specific surface area close to the surface on the Antarctic Plateau, *The Cryosphere*, 9, 2383-2398, 2015.

934 Lorius, C., Jouzel, J., Ritz, C., Merlivat, L., Barkov, N. I., Korotkevich, Y. S., and Kotlyakov, V. M.: A 150,000-year  
935 climatic record from Antarctic ice, *Nature*, 316, 591-596, 1985.

936 Lu, G. and DePaolo, D. J.: Lattice Boltzmann simulation of water isotope fractionation during ice crystal growth in  
937 clouds, *Geochimica et Cosmochimica Acta*, 180, 271-283, 2016.

938 Mann, M. E. and Jones, P. D.: Global surface temperatures over the past two millennia, *Geophysical Research Letters*,  
939 30, 1820, doi:10.1029/2003GL017814, 2003.

940 Masson-Delmotte, V., Landais, A., Stievenard, M., Cattani, O., Falourd, S., Jouzel, J., Johnsen, S. J., Dahl-Jensen, D.,  
941 Sveinsbjörnsdóttir, A., White, J. W. C., Popp, T., and Fischer, H.: Holocene climatic changes in Greenland: Different  
942 deuterium excess signals at Greenland Ice Core Project (GRIP) and NorthGRIP, *Journal of Geophysical Research:*  
943 *Atmospheres*, 110, 1-13, 2005.

944 Masson-Delmotte, V., Buiron, D., Ekaykin, A., Frezzotti, M., Gallée, H., Jouzel, J., Krinner, G., Landais, A.,  
945 motoyama, H., Oerter, H., Pol, K., Pollard, D., Ritz, C., Schlosser, Z., Sime, L. C., Sodemann, H., Stenni, B., Uemura,  
946 R., and Vimeux, F.: A comparison of the present and last interglacial periods in six Antarctic ice cores, *Clim. Past*, 7,  
947 397-423, 2011.

948 Masson-Delmotte, V., Steen-Larsen, H., Ortega, P., Swingedouw, D., Popp, T., Vinther, B., Oerter, H.,  
949 Sveinbjörnsdóttir, A., Gudlaugsdóttir, H., and Box, J.: Recent changes in north-west Greenland climate documented  
950 by NEEM shallow ice core data and simulations, and implications for past-temperature reconstructions, *The*  
951 *Cryosphere* 9, 1481-1504, 2015.

952 Morse, D. L., Waddington, E. D., Marshall, H.-P., Neumann, T. A., Steig, E. J., Dibb, J. E., Winebrenner, D. P., and  
953 Arthern, R. J.: Accumulation Rate Measurements at Taylor Dome, East Antarctica: Techniques and Strategies for Mass  
954 Balance Measurements in Polar Environments, *Geografiska Annaler: Series A, Physical Geography*, 81, 683-694,  
955 1999.

956 Neumann, T. A.: Effects of firn ventilation on geochemistry of polar snow, PhD, Department of Earth and Space  
957 Sciences, University of Washington, Washington, 223 pp., 2003.

958 Neumann, T. A. and Waddington, E. D.: Effects of firn ventilation on isotopic exchange, *Journal of Glaciology*, 50,  
959 183-194, 2004.

960 Neumann, T. A., Waddington, E. D., Steig, E. J., and Grootes, P. M.: Non-climate influences on stable isotopes at  
961 Taylor Mouth, Antarctica, *Journal of Glaciology*, 51, 248-258, 2005.

962 Neumann, T., Albert, M., Lomonaco, R., Engel, C., Courville, Z., and Perron, F.: Experimental determination of snow  
963 sublimation rate and stable-isotopic exchange, *Annals of Glaciology*, 49, 1-6, 2008.

964 Neumann, T. A., Albert, M. R., Engel, C., Courville, Z., and Perron, F.: Sublimation rate and the mass-transfer  
965 coefficient for snow sublimation, *International Journal of Heat and Mass Transfer*, 52, 309-315, 2009.

966 Petit, J. R., Jouzel, J., Pourchet, M., and Merlivat, L.: A detailed study of snow accumulation and stable isotope content

967 in Dome C (Antarctica), *Journal of Geophysical Research*, 87, 4301-4308, 1982.

968 Petit, J. R., Jouzel, J., Raynaud, D., Barkov, N. I., Barnola, J. M., Basile, I., Bender, M., Chappellaz, J., Davis, M.,  
969 Delaygue, G., Delmotte, M., Kotlyakov, V. M., Legrand, M., Lipenkov, V. Y., Lorius, C., Pepin, L., Ritz, C., Saltzman,  
970 E., and Stievenard, M.: Climate and atmospheric history of the past 420,000 years from the Vostok ice core, Antarctica,  
971 *Nature*, 399, 429-436, 1999.

972 Pinzer, B. R., Schneebeli, M., and Kaempfer, T. U.: Vapor flux and recrystallization during dry snow metamorphism  
973 under a steady temperature gradient as observed by time-lapse micro-tomography, *The Cryosphere*, 6, 1141-1155,  
974 2012.

975 Ramseier, R. O.: Self-diffusion of tritium in natural and syntehtic ice monocrystals, *Journal of Applied Physics*, 38,  
976 2553-2556, 1967.

977 Ritter, F., Steen-Larsen, H. C., Werner, M., Masson-Delmotte, V., Orsi, A., Behrens, M., Birnbaum, G., Freitag, J.,  
978 Risi, C., and Kipfstuhl, S.: Isotopic exchange on the diurnal scale between near-surface snow and lower atmospheric  
979 water vapor at Kohnen station, East Antarctica, *The Cryosphere Discuss.*, 2016, 1-35, 2016.

980 Schneider, D. P., Steig, E. J., Ommen, T. D. v., Dixon, D. A., Mayewski, P. A., Jones, J. M., and Bitz, C. M.: Antarctic  
981 temperatures over the past two centuries from ice cores, *Geophysical Research Letters*, 33, L16707, 2006.

982 Shaheen, R., Abauanza, M., Jackson, T. L., McCabe, J., Savarino, J., and Thiemens, M. H.: Tales of volcanoes and El-  
983 Niño southern oscillations with the oxygen isotope anomaly of sulfate aerosol, *Proceedings of the National Academy*  
984 *of Sciences*, 110, 17662-17667, 2013.

985 Shuman, C. A., Alley, R. B., Anandakrishnan, S., White, J. W. C., Grootes, P. M., and Stearns, C. R.: Temperature  
986 and accumulation at the Greenland Summit: Comparison of high-resolution isotope profiles and satellite passive  
987 microwave brightness temperature trends, *Journal of Geophysical Research: Atmospheres*, 100, 9165-9177, 1995.

988 Shuman, C. A., Steffen, K., Box, J. E., and Stearns, C. R.: A dozen years of temperature observations at the Summit:  
989 Central Greenland automatic weather stations 1987–99, *Journal of Applied Meteorology*, 40, 741-752, 2001.

990 Sime, L. C., Tindall, J. C., Wolff, E. W., Connolley, W. M., and Valdes, P. J.: Antarctic isotopic thermometer during  
991 a CO2 forced warming event, *Journal of Geophysical Research*, 113, D24119, 2008.

992 Sjolte, J., Hoffmann, G., Johnsen, S. J., Vinther, B. M., Masson-Delmotte, V., and Sturm, C.: Modeling the water  
993 isotopes in Greenland precipitation 1959–2001 with the meso-scale model REMO-iso, *Journal of Geophysical*

994 Research: Atmospheres, 116, D18105, doi:10.1029/2010JD015287, 2011.

995 Sokratov, S. A. and Golubev, V. N.: Snow isotopic content change by sublimation, *Journal of Glaciology*, 55, 823-  
996 828, 2009.

997 Steen-Larsen, H. C., Masson-Delmotte, V., Sjolte, J., Johnsen, S. J., Vinther, B. M., Bréon, F. M., Clausen, H., Dahl-  
998 Jensen, D., Falourd, S., and Fettweis, X.: Understanding the climatic signal in the water stable isotope records from  
999 the NEEM shallow firn/ice cores in northwest Greenland, *Journal of Geophysical Research: Atmospheres*, 116,  
1000 D06108, doi:10.1029/2010JD014311, 2011.

1001 Steen-Larsen, H., Masson-Delmotte, V., Hirabayashi, M., Winkler, R., Satow, K., Prié, F., Bayou, N., Brun, E., Cuffey,  
1002 K., and Dahl-Jensen, D.: What controls the isotopic composition of Greenland surface snow?, *Climate of the Past*, 10,  
1003 377-392, 2014.

1004 Steig, E. J.: The south-north connection, *Nature*, 44, 152-153, 2006.

1005 Stenni, B., Jouzel, J., Masson-Delmotte, V., Röthlisberger, R., Castellano, E., Cattani, O., Falourd, S., Johnsen, S. J.,  
1006 Longinelli, A., Sachs, J. P., Selmo, E., Souchez, R., Steffensen, J. P., and Udisti, R.: A late-glacial high-resolution site  
1007 and source temperature record derived from the EPICA Dome C isotope records (East Antarctica), *Earth and Planetary  
1008 Science Letters*, 217, 183-195, 2004.

1009 Stenni, B., Buiron, D., Frezzotti, M., Albani, S., Barbante, C., Bard, E., Barnola, J. M., Baroni, M., Baumgartner, M.,  
1010 Bonazza, M., Capron, E., Castellano, E., Chappellaz, J., Delmonte, B., Falourd, S., Genoni, L., Iacumin, P., Jouzel, J.,  
1011 Kipfstuhl, S., Landais, A., Lemieux-Dudon, B., Maggi, V., Masson-Delmotte, V., Mazzola, C., Minster, B.,  
1012 Montagnat, M., Mulvaney, R., Narcisi, B., Oerter, H., Parrenin, F., Petit, J. R., Ritz, C., Scarchilli, C., Schilt, A.,  
1013 Schupbach, S., Schwander, J., Selmo, E., Severi, M., Stocker, T. F., and Udisti, R.: Expression of the bipolar see-saw  
1014 in Antarctic climate records during the last deglaciation, *Nature Geosci*, 4, 46-49, 2011.

1015 Stenni, B., Scarchilli, C., Masson-Delmotte, V., Schlosser, E., Ciardini, V., Dreossi, G., Grigioni, P., Bonazza, M.,  
1016 Cagnati, A., Karlicek, D., Risi, C., Udisti, R., and Valt, M.: Three-year monitoring of stable isotopes of precipitation  
1017 at Concordia Station, East Antarctica, *The Cryosphere*, 10, 2415-2428, 2016.

1018 Stichler, W., Schotterer, U., Fröhlich, K., Ginot, P., Kull, C., Gäggeler, H., and Pouyau, B.: Influence of sublimation  
1019 on stable isotope records recovered from high-altitude glaciers in the tropical Andes, *Journal of Geophysical Research*,  
1020 106, 22613-22620, 2001.

1021 Touzeau, A., Landais, A., Stenni, B., Uemura, R., Fukui, K., Fujita, S., Guilbaud, S., Ekaykin, A., Casado, M., and  
1022 Barkan, E.: Acquisition of isotopic composition for surface snow in East Antarctica and the links to climatic  
1023 parameters, *The Cryosphere*, 10, 837-852, 2016.

1024 Town, M. S., Warren, S. G., Walden, V. P., and Waddington, E. D.: Effect of atmospheric water vapor on modification  
1025 of stable isotopes in near-surface snow on ice-sheets, *Journal of Geophysical Research*, 113, D24303, 2008.

1026 Uemura, R., Landais, A., Motoyama, H., and Stenni, B. : Ranges of moisture-source temperature estimated from  
1027 Antarctic ice cores stable isotope records over glacial-interglacial cycles, *Climate of the Past*, 8, 1109-1025, 2012.

1028 Urbini, S., Frezzotti, M., Gandolfi, S., Vincent, C., Scarchilli, C., Vittuari, L., and Fily, M.: Historical behaviour of  
1029 Dome C and Talos Dome (East Antarctica) as investigated by snow accumulation and ice velocity measurements,  
1030 *Global and Planetary Change*, 60, 576-588, 2008.

1031 van de Berg, W. J., van den Broeke, M. R., Reijmer, C. H., and van Meijgaard, E.: Reassessment of the Antarctic  
1032 surface mass balance using calibrated output of a regional atmospheric climate model, *Journal of Geophysical  
1033 Research: Atmospheres*, 111, D11104, doi:10.1029/2005JD006495, 2006.

1034 van der Wel, L., Been, H., Smeets, P., and Meijer, H.: Constraints on the  $\delta^2\text{H}$  diffusion rate in firn from field  
1035 measurements at Summit, Greenland, *The Cryosphere*, 9, 1089-1103, 2015.

1036 Vionnet, V., Brun, E., Morin, S., Boone, A., Faroux, S., Le Moigne, P., Martin, E., and Willemet, J.: The detailed  
1037 snowpack scheme Crocus and its implementation in SURFEX v7. 2, *Geoscientific Model Development*, 5, 773-791,  
1038 2012.

1039 Waddington, E. D., Steig, E. J., and Neumann, T. A.: Using characteristic times to assess whether stable isotopes in  
1040 polar snow can be reversibly deposited, *Annals of Glaciology*, 35, 118-124, 2002.

1041 WAIS Divide Project Members: Onset of deglacial warming in West Antarctica driven by local orbital forcing, *Nature*,  
1042 500, 440-444, 2013.

1043 White, J.W.C., Barlow, L.K., Fisher, D., Grootes, P., Jouzel, J., Johnsen, S.J., Stuiver, M., and Clausen, H.: The climate  
1044 signal in the stable isotope of Summit, Greenland snow : Results of comparisons with modern climate observations.  
1045 *Journal of Geophysical Research*, 102, C12, 26425 - 26439, 1997.

1046

1047 **Table 1.** Definition of the symbols used.

Symbol	Description
<b>Constants</b>	
$T_0$	Temperature of the triple point of water (K)
$R_v$	Vapor constant for water ( $J \cdot kg^{-1} K^{-1}$ )
$L_{sub}$	Latent heat of sublimation of water ( $J \cdot m^{-3}$ )
$C_{v0}$	Vapor mass concentration at 273.16 K ( $kg \cdot m^{-3}$ of air)
$D_{ice}$	Diffusivity of water molecules in solid ice ( $m^2 \cdot s^{-1}$ )
$D_v$	Diffusivity of vapor in air at 263 K ( $m^2 \cdot s^{-1}$ ) (temperature dependency neglected)
$\rho_{ice}$	Density of ice ( $kg \cdot m^{-3}$ )
$A$	Accumulation (m i.e. per year)
$R_{moy}$	Average snow grain radius (m)
$\Delta t_{sol}$	Characteristic time for solid diffusion (s)
$\Delta t_{surf/center}$	Periodicity of the mixing between grain center and grain surface, because of grain center translation (s)
<b>1D-variables</b>	
$T$	Time (s)
$N$	Layer number from top of the snowpack
$\delta^{18}O_{sf}(t)$	Isotopic composition of oxygen in the snowfall (‰)
$T_{air}(t)$	Temperature of the air at 2 m (K)
<b>2D-variables</b>	
$h(t,n)$	Height of the center of the snow layer relative to the bottom of the snowpack (m)
$z(t,n)$	Depth of the center of the snow layer (m from surface)
$dz(t,n)$	Thickness of the snow layer (m)
$T(t,n)$	Temperature of the snow layer (K)
$\rho_{sn}(t,n)$	Density of the snow layer ( $kg \cdot m^{-3}$ )
$m_{sn}(t,n)$	Mass of the snow layer (kg)
$C_v(t,n)$	Vapor mass concentration at saturation in the porosity of the snow layer ( $kg \cdot m^{-3}$ of air)
$D_{eff}(t,n)$	Effective diffusivity of vapor in the layer ( $m^2 \cdot s^{-1}$ )
$\delta^{18}O(t,n)$	Isotopic composition of oxygen in the snow layer (‰)
$F^{18}(n+1 \rightarrow n)$	Flux of the heavy water molecules ( $^{18}O$ ) from layer $n+1$ to layer $n$ ( $kg \cdot m^{-2} \cdot s^{-1}$ )
$F(n+1 \rightarrow n)$	Vapor flux from layer $n+1$ to layer $n$ ( $kg \cdot m^{-2} \cdot s^{-1}$ )
$D_{eff}(t,n \rightarrow n+1)$	Effective interfacial diffusivity between layers $n$ and $n+1$ ( $m^2 \cdot s^{-1}$ )
$R_{vap\ ini}^i$	Isotopic ratio in the initial vapor ( $i$ is either $^{18}O$ , $^{17}O$ or $D$ )
$R_{surf\ ini}^i$	Isotopic ratio in the grain surface sub-compartment before vapor individualization
$c_{vap\ ini}^x$	Ratio between the mass of a given isotopologue in the initial vapor ( $x$ is $^{18}O$ , $^{17}O$ , $^{16}O$ , $^1H$ or $D$ ) and the total mass of vapor (no unit). The mass balance is made separately and independently for $H$ and $O$ (i.e.: $c_{vap\ ini}^{18} + c_{vap\ ini}^{17} + c_{vap\ ini}^{16} = 1$ and $c_{vap\ ini}^{1H} + c_{vap\ ini}^D = 1$ ).
$\alpha_{sub}^i$	Fractionation coefficients at equilibrium during sublimation ( $i$ is either $^{18}O$ , $^{17}O$ or $D$ ) Fractionation coefficients during condensation ( $i$ is either $^{18}O$ , $^{17}O$ or $D$ )
$\alpha_{cond}^i$	No fractionation
$\alpha_{cond\ eff}^i$	Effective (total) fractionation

$\alpha_{cond\ kin}^i$	Kinetic fractionation only
$\alpha_{cond\ eq}^i$	Equilibrium fractionation only
$m_{vap\ ini}$	Initial mass of vapor in the porosity (kg)
$m_{surf\ ini}$	Mass of water in the grain surface sub-compartment before vapor individualization (kg)
$m_{surf\ new}$	Mass of water in the grain surface sub-compartment after vapor individualization (kg)
$T$	Ratio of between the mass of the grain surface compartment and the mass of total grain
$m_{surf}$	Mass of grain surface compartment
$m_{center}$	Mass of grain center compartment
$m_{vap}$	Mass of vapor in the porosity
$V_{tot}$	Total volume of the considered layer
$\Phi$	Porosity of the layer
$m_{surf\ ini}^{18}$	Mass of heavy water molecules ( $^{18}\text{O}$ ) in the grain surface before vapor individualization (kg)
$m_{surf\ new}^{18}$	Mass of heavy water molecules ( $^{18}\text{O}$ ) in the grain surface after vapor individualization (kg)
$D^{18}/D$	Ratio of diffusivities between heavy isotope and light isotope
$\Delta m_{vap,exc}$	Mass of vapor in excess in the porosity after vapor transport (kg)
$\rho_{sn\ ini}$	Density of the snow layer before vapor transport
$\rho_{sn\ new}$	Density of the snow layer after vapor transport
$T_{ini}, T_{new}$	Temperature of the snow layer before and after vapor transport

---

1048

1049

<b>GRIP</b>		
Accumulation	23 cm i.e. yr. <sup>-1</sup>	Dahl-Jensen et al., 1993
Annual temperature	241 K	Masson-Delmotte et al., 2005
Winter temperature	232 K	(Feb.) Shuman et al., 2001
Summer temperature	261 K	(Aug.) Shuman et al., 2001
Mean $\delta^{18}\text{O}$	-35.2‰	Masson-Delmotte et al., 2005
$\delta^{18}\text{O}$ min	-43 ‰	(2m snow pit) Shuman et al., 1995
$\delta^{18}\text{O}$ max	-27 ‰	(2m snow pit) Shuman et al., 1995
$\delta^{18}\text{O}/\text{T}$ slope	0.46 ‰/°C	(2m snow pit) Shuman et al., 1995
<b>DOME C</b>		
Accumulation	2.7 cm i.e. yr. <sup>-1</sup>	Frezzotti et al., 2005; Urbini et al., 2008
Annual temperature	221 K	Stenni et al., 2016
Min winter T	199 K	Stenni et al., 2016
Max summer T	248 K	Stenni et al., 2016
Mean $\delta^{18}\text{O}$	-56.4 ‰	Stenni et al., 2016
$\delta^{18}\text{O}$ min winter	-71.8 ‰	Stenni et al., 2016
$\delta^{18}\text{O}$ max summer	-40.2 ‰	Stenni et al., 2016
$\delta^{18}\text{O}/\text{T}$ slope	0.49 ‰/°C	Stenni et al., 2016

1050 **Table 2.** Climate and isotope variability at GRIP (Greenland) and Dome C (Antarctica).

1051

1052

Variable	Equation	Average	Range	
Thickness (m)	$dz$	$1.2 \cdot 10^{-1}$	$5 \cdot 10^{-4}$	$8 \cdot 10^{-1}$
Density ( $\text{kg m}^{-3}$ )	$\rho_{\text{sn}}$	340	300	460
Temperature (K)	$T$	225	205	255
Mass (kg)	$m_{\text{sn}} = dz \cdot \rho_{\text{sn}}$	42	0.15	368
Vapor mass concentration ( $\text{kg} \cdot \text{m}^{-3}$ )	$C_v$ Eq. (8)	$1.8 \cdot 10^{-5}$	$1.2 \cdot 10^{-6}$	$4.4 \cdot 10^{-4}$
Porosity	$\Phi = 1 - (\rho_{\text{sn}} / \rho_{\text{ice}})$	0.63	0.5	0.67
Vapor mass (kg)	$m_{\text{vap}}$ Eq. (11)	$1.3 \cdot 10^{-6}$	$3 \cdot 10^{-10}$	$2.4 \cdot 10^{-4}$
Minimum ratio	$\tau_{\text{min}} = 1/10^6$	$1 \cdot 10^{-6}$	$1 \cdot 10^{-6}$	$1 \cdot 10^{-6}$
Maximum ratio	$\tau_{\text{max}} = \frac{C_v \cdot \Phi}{\rho_{\text{sn}}} \cdot 10^6$	$3.3 \cdot 10^{-2}$	$1.3 \cdot 10^{-3}$	1

1053  
1054 **Table 3.** Typical thickness, density, temperature and other parameters of the snow layers in the simulations. The ratio  
1055  $\tau$  is the mass ratio between the grain surface compartment and the grain center compartment. It must be chosen within  
1056 the interval [ $10^{-6}$  ;  $10^6$  ( $C_v \Phi / \rho_{\text{sn}}$ )] to allow exchanges between grain surface compartment and grain center  
1057 compartment, on the one hand; and between grain surface compartment and vapor compartment on the other hand (see  
1058 text for details).

	GRIP simulation			Dome C simulations		
N°	1	2	3	4	5	6
Section	4.1.1.	4.1.2.	4.2.1.	4.2.2.	4.2.3.	4.2.4.
Figures	Figure 2	Figure 3	Figure 5	Figure 6	Figure 7	Figure 8
Duration	10 years	10 years	1 year	1 year	1 year	10 years
Period	Jan 2000- Dec 2010	Jan 2001- Dec 2011	Jan- Dec 2001	Jan- Dec 2001	Jan- Dec 2001	Jan 2000- Dec 2010
<i>Atmospheric forcing applied</i>						
Air T	-	ERA-Interim (GR)	ERA-Interim	ERA-Interim	ERA-Interim	ERA-Interim
Specific humidity	-	ERA-Interim (GR)	ERA-Interim	ERA-Interim	ERA-Interim	ERA-Interim
Air pressure	-	ERA-Interim (GR)	ERA-Interim	ERA-Interim	ERA-Interim	ERA-Interim
Wind velocity	-	ERA-Interim (GR)	ERA-Interim	ERA-Interim	ERA-Interim	ERA-Interim
Snowfall	NO	NO	NO	NO	YES	YES
$\delta^{18}\text{O}_{\text{sf}}$	-	-	-	-	Function (T)*	Function (T)*
<i>Model configuration</i>						
Initial snow T	Flat profile (241 K)	One-year run initialization (Jan-Dec 2000)	One-year run initialization (Jan-Dec 2000)	One-year run initialization (Jan-Dec 2000)	One-year run initialization (Jan-Dec 2000)	Exponential profile**
Evolution of snow T	Constant	Computed	Computed	Computed	Computed	Computed
Initial snow d18O	Sinusoidal profile***	Sinusoidal profile***	-40 ‰	-40 ‰	-40 ‰	-40 ‰
Wind drift	NO	NO	NO	YES	YES	NO
Homogeneous compaction	NO	NO	NO	YES	YES	NO

1059

1060 Table 4. List of simulations described in the article with the corresponding paragraph number. The external atmospheric forcing used for Dome C is ERA-Interim

1061 reanalysis (2000-2013). However, the precipitation amounts from ERA-Interim reanalysis are increased by 1.5 times to account for the dry bias in the reanalysis

1062 (as in Libois et al., 2014). For the second simulation at GRIP, Greenland meteorological conditions are derived from the atmospheric forcing of Dome C, but the

1063 temperature is modified ( $T_{\text{GRIP}}=T_{\text{DC}}+15$ ) as well as the longwave down ( $LW_{\text{GRIP}}=0.85 LW_{\text{DC}} +60$ ).

1064 \* Using data from one-year snowfall sampling at Dome C (Stenni et al., 2016; Touzeau et al., 2016), we obtained the following Eq. (16) linking  $\delta^{18}\text{O}$  in the snowfall

1065 to the local temperature:  $\delta^{18}O_{sf} = 0.45 \times (T - 273.15) - 31.5$ .

1066 \*\*The exponential profile of temperature used in simulation 6 is defined using Eq. (20):

$$1067 \quad T(z) = T(10m) + \Delta T \times \exp(-z/z_0) + 0.1 \times z \quad (20)$$

1068 with  $T(10m)=218$  K,  $\Delta T=28$  K, and  $z_0=1.516$  m.

1069 It fits well with temperature measurements of midday in January (Casado et al., 2016b).

1070 \*\*\*The Greenland snowpack has an initial sinusoidal profile of  $\delta^{18}\text{O}$  defined using Eq. (19):  $\delta^{18}O = -35.5 - 8 \times \sin\left(\frac{2\pi \times z}{a \times \rho_{ice} / \rho_{sn}}\right)$

1071

1072

1073

	GRIP sensitivity tests				Dome C sensitivity tests				
N°	1	2	3	4	1	2	3	4	5
Section	4.3.	4.3.	4.3.	4.3.	4.3.	4.3.	4.3.	4.3.	4.3.
Figures	Figure 9	Figure 9	Figure 9	Figure 9	Figure 10	Figure 10	Figure 10	Figure 10	Figure 10
Duration	6 months	6 months	6 months	6 months	3 years	3 years	3 years	3 years	3 years
Period	Jan-Jun 2000	Jan-Jun 2000	Jan-Jun 2000	Jan-Jun 2000	Jan 2000-Dec 2002	Jan 2000-Dec 2002	Jan 2000-Dec 2002	Jan 2001-Dec 2003	Jan 2001-Dec 2003
<i>Atmospheric forcing applied</i>									
Air T	-	-	-	-	-	-	-	ERA-Interim	ERA-Interim
Specific humidity	-	-	-	-	-	-	-	ERA-Interim	ERA-Interim
Air pressure	-	-	-	-	-	-	-	ERA-Interim	ERA-Interim
Wind velocity	-	-	-	-	-	-	-	ERA-Interim	ERA-Interim
Snowfall	NO	NO	NO	NO	NO	NO	NO	NO	NO
$\delta^{18}\text{O}_{\text{sf}}$	-	-	-	-	-	-	-	-	-
<i>Model configuration</i>									
Initial snow T	Flat profile (241 K)	Flat profile (241 K)	Flat profile (241 K)	Flat profile (241 K)	Flat profile (241 K)	Flat profile (220 K)	Flat profile (220 K)	One-year run initialization (Jan-Dec 2000)	One-year run initialization (Jan-Dec 2000)
Evolution of snow T	Constant	Constant	Constant	Constant	Constant	Constant	Constant	Computed	Computed
Initial snow d18O	Sinusoidal profile***	Sinusoidal profile***	Sinusoidal profile***	Sinusoidal profile***	Sinusoidal profile****	Sinusoidal profile****	Sinusoidal profile****	Sinusoidal profile****	Sinusoidal profile****
Wind drift	NO	NO	NO	NO	NO	NO	NO	NO	NO
Homogeneous compaction	NO	NO	NO	NO	NO	NO	NO	NO	NO
Mass ratio $\tau$ within the grain	$1 \cdot 10^{-6}$	$5 \cdot 10^{-4}$	$3.3 \cdot 10^{-2}$	$5 \cdot 10^{-4}$	$5 \cdot 10^{-4}$	$5 \cdot 10^{-4}$	$5 \cdot 10^{-4}$	$5 \cdot 10^{-4}$	$3.3 \cdot 10^{-2}$

Period for recrystallization $\Delta t_{surf/center}$	15 days	15 days	15 days	2 days	15 days	2 days	15 days	15 days	15 days
--	---------	---------	---------	--------	---------	--------	---------	---------	---------

---

1074

1075 Table 5. List of the sensitivity tests performed at GRIP and at Dome C. The external atmospheric forcing used for Dome C is ERA-Interim reanalysis (see Table 4).

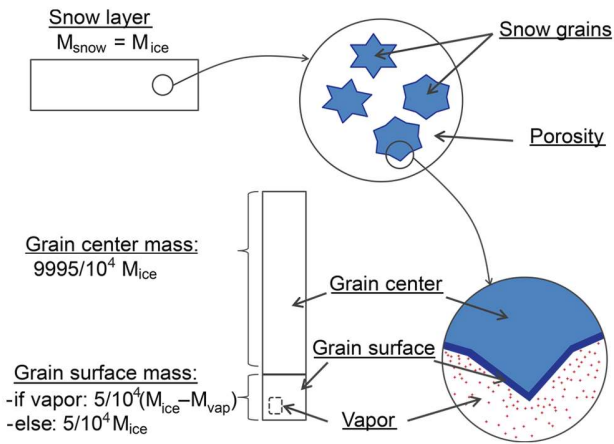
1076 \*\*\*The Greenland snowpack has an initial sinusoidal profile of  $\delta^{18}O$  defined using Eq. (19):

1077 
$$\delta^{18}O = -35.5 - 8 \times \sin\left(\frac{2\pi \times z}{a \times \rho_{ice} / \rho_{sn}}\right)$$

1078 \*\*\*\*The Dome C snowpack has an initial sinusoidal profile of  $\delta^{18}O$  defined using Eq. (21):

1079 
$$\delta^{18}O = -48.5 - 6.5 \times \sin\left(\frac{2\pi \times z}{a \times \rho_{ice} / \rho_{sn}}\right) \quad (21)$$

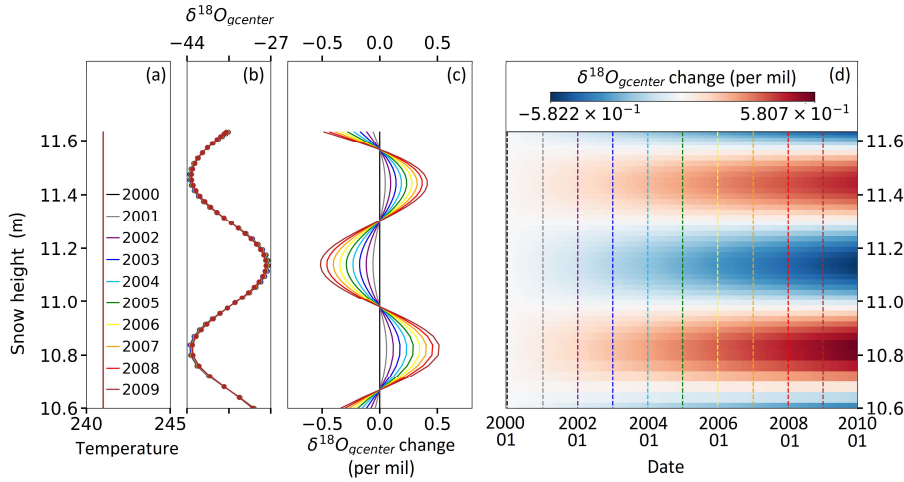
1080



1081  
1082  
1083  
1084  
1085

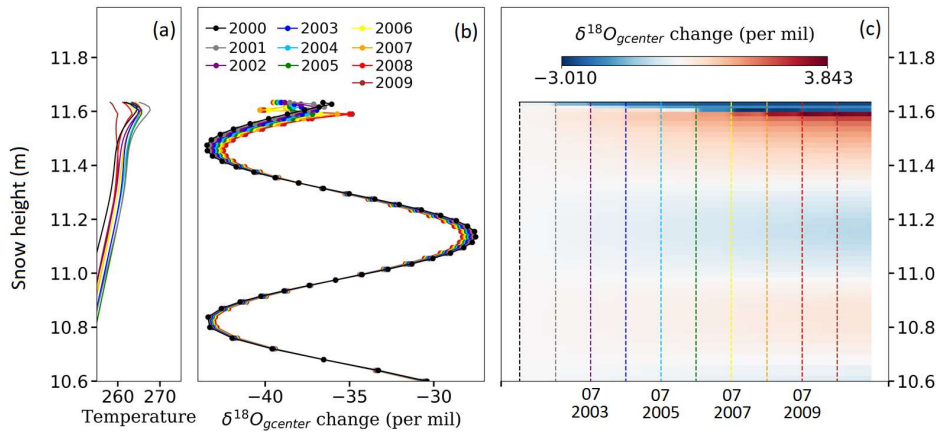
**Figure 1.** Splitting of the snow layer into two compartments, grain center and grain surface, with a constant mass ratio between them. The vapor compartment is a sub-compartment inside the grain surface compartment and is only defined at specific steps of the model.

1086



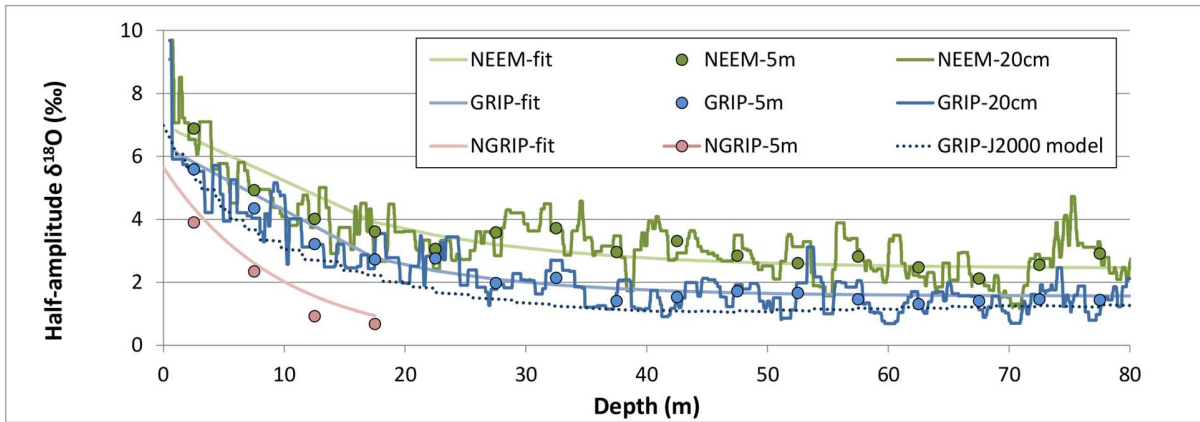
1087  
 1088 **Figure 2. Simulation 1:** Attenuation of the seasonal  $\delta^{18}\text{O}_{gcenter}$  variation caused by diffusion along isotopic gradients  
 1089 in vapor phase over 10 years (homogeneous and constant temperature of 241 K, original signal with mean value of -  
 1090 35.5 ‰ and amplitude of 16 ‰). (a) Vertical homogeneous temperature profile; (b)  $\delta^{18}\text{O}$  profile at the beginning and  
 1091 end of the simulation; (c) Deviation of the  $\delta^{18}\text{O}$  relative to the original profile, for 10 dates; (d) Evolution of the  
 1092 deviation to the original profile of  $\delta^{18}\text{O}$ .

1093  
 1094



1095  
 1096 **Figure 3. Simulation 2:** Attenuation of the seasonal  $\delta^{18}\text{O}_{gcenter}$  variation caused by diffusion in vapor phase over 10  
 1097 years (with temperature evolution, original signal with mean value of -35.5 ‰ and amplitude of 16 ‰). (a) Vertical  
 1098 temperature profile for each summer; (b)  $\delta^{18}\text{O}_{gcenter}$  profile for each summer; (c) Evolution of the deviation to the  
 1099 original profile of  $\delta^{18}\text{O}_{gcenter}$ . Note that temperature evolves during the whole year (see Fig. S1).

1100



1101

1102 **Figure 4.** Evolution of the  $\delta^{18}\text{O}$  semi-amplitude with depth in shallow cores at NEEM, GRIP and NGRIP (Steen-  
 1103 Larsen et al., 2011 and Masson-Delmotte et al., 2015; White et al., 1997; Johnsen et al., 2000). The attenuation of  
 1104 the semi-amplitude values with depth was fitted using an exponential equation (Eq. (22)):

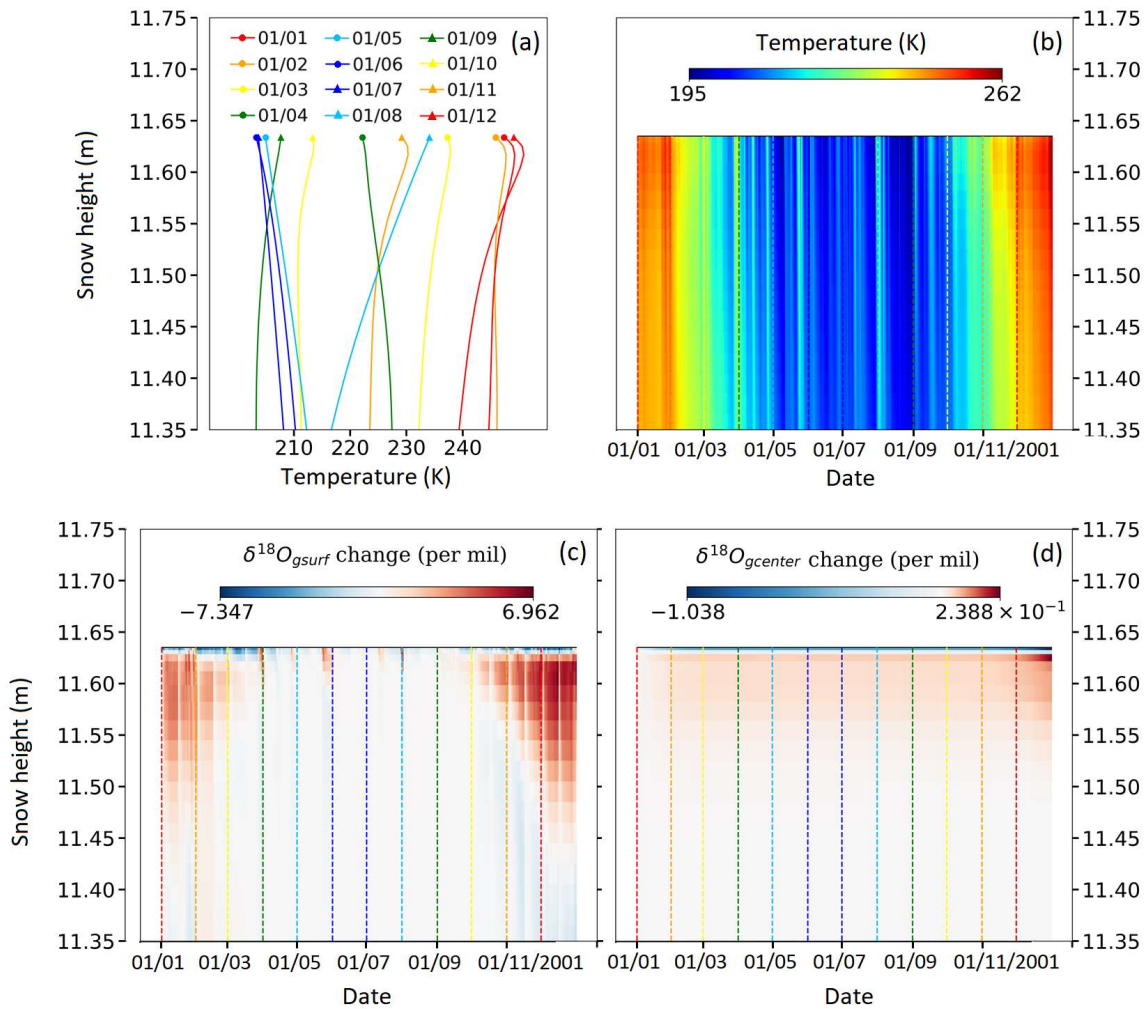
1105 
$$A = A_0 \cdot \exp(-\gamma \cdot z) - b \tag{22}$$

1106 With  $A_0=4.976 \text{ ‰}$ ;  $\gamma=0.08094$ ;  $b=-1.56 \text{ ‰}$  at GRIP, and  $A_0=4.685 \text{ ‰}$ ;  $\gamma=0.06622$ ;  $b=-2.44 \text{ ‰}$  at NEEM.

1107 The dotted curve corresponds to the simulated attenuation at GRIP based on the Johnsen et al.'s model (diffusion  
 1108 length  $\sigma$  from their Figure 2, and wavelength  $\lambda$  fitted on the Eurocore core from GRIP, White et al., 1997).

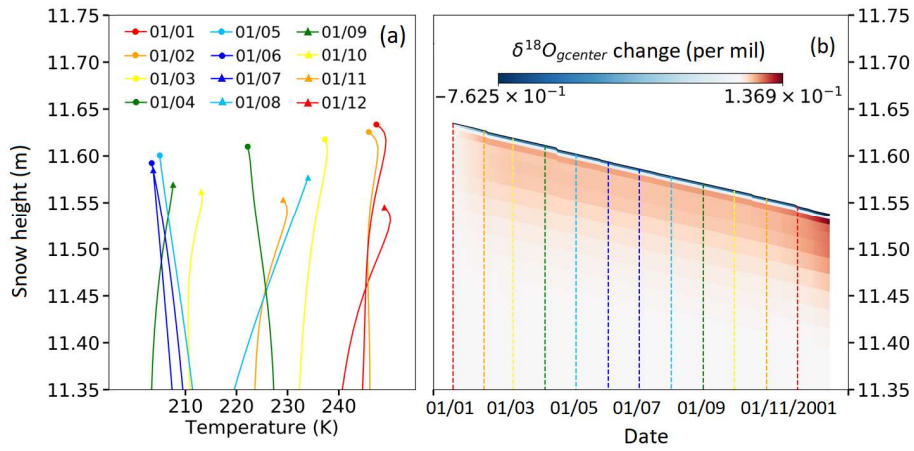
1109

1110  
1111



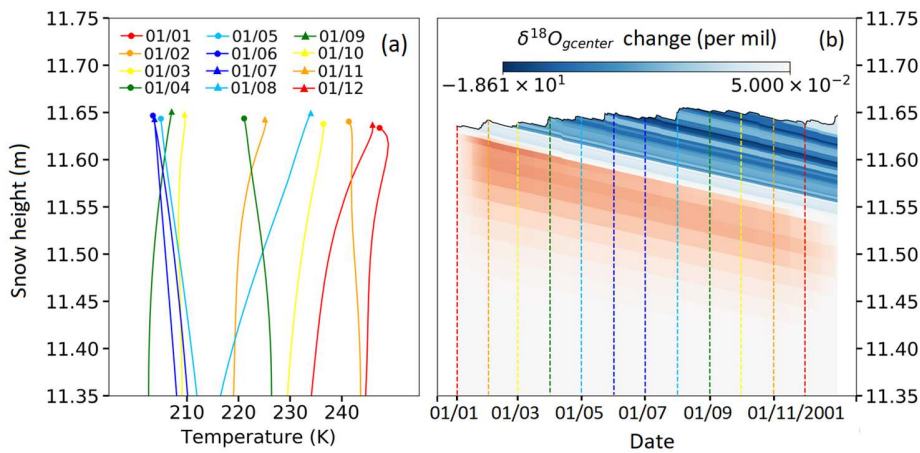
1112  
1113  
1114  
1115  
1116  
1117  
1118  
1119  
1120  
1121  
1122

**Figure 5.** Simulation 3: Evolution of temperature and  $\delta^{18}\text{O}$  values from January to December 2001. (a) Temperature profiles for the first day of each month; (b) Temperature evolution in the snowpack; (c) ' $\delta^{18}\text{O}$  change' in the grain surface compartment; (d) ' $\delta^{18}\text{O}$  change' in the grain center compartment. Here, ' $\delta^{18}\text{O}$  change' stands for the difference between  $\delta^{18}\text{O}$  at  $t$  and at the beginning of the simulation for the selected layer.

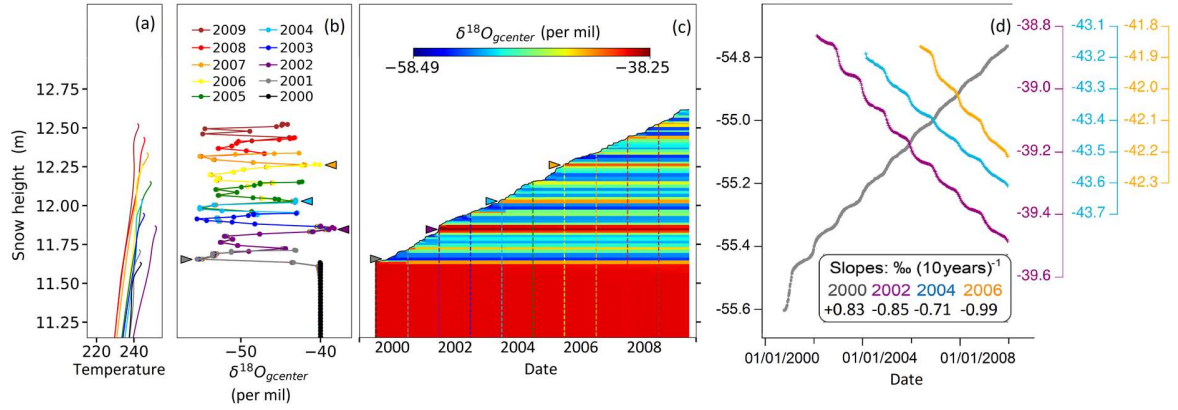


1123  
 1124 **Figure 6. Simulation 4:** Cumulative change in  $\delta^{18}\text{O}_{gcenter}$  values (vapor transport, compaction and wind drift active).  
 1125

1126  
 1127  
 1128

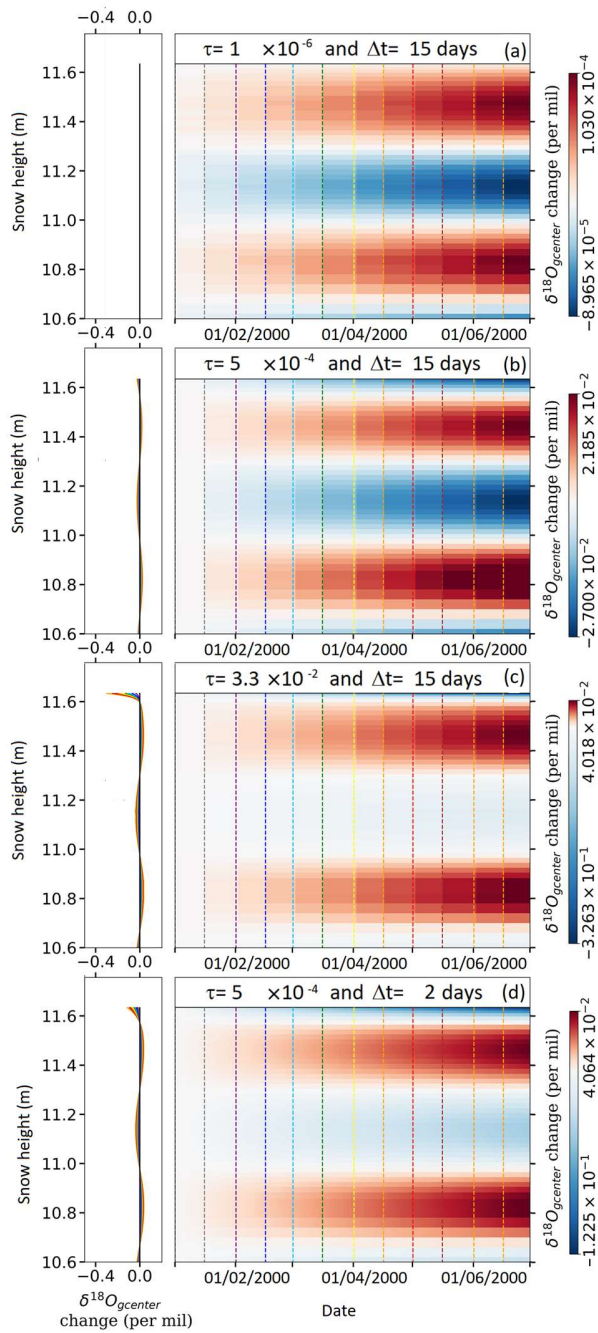


1129  
 1130 **Figure 7. Simulation 5:** Cumulative change of  $\delta^{18}\text{O}$  values at the grain center (relative to  $t_0$ ) over 6 months.  
 1131 Simulation with snowfall with varying  $\delta^{18}\text{O}$  (function of  $T_{air}$ ), vapor transport active, wind and weight compaction  
 1132 active.  
 1133



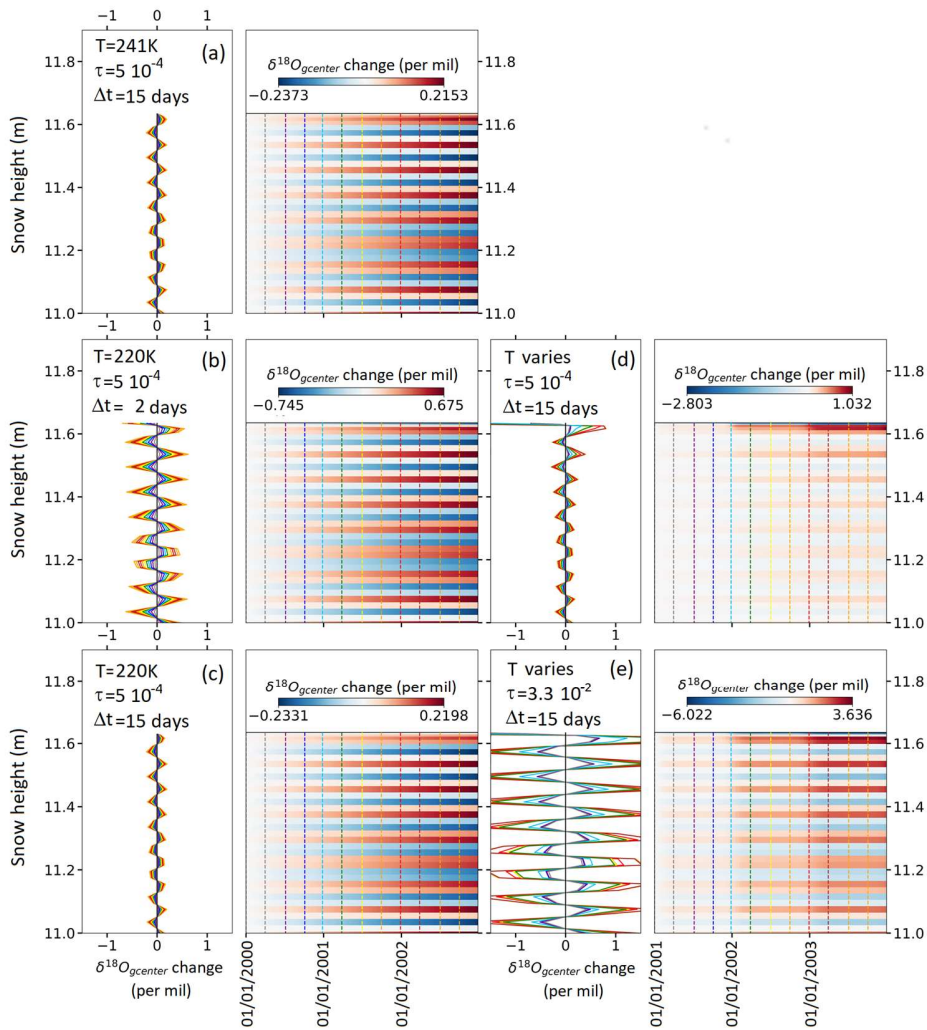
1134  
 1135 **Figure 8. Simulation 6:** Evolution of  $\delta^{18}\text{O}_{\text{gcenter}}$  values as a result of snowfall and vapor transport over 10 years  
 1136 (compaction is inactive; merging between layers is allowed but limited). (a) Temperature profiles at mid-January for  
 1137 each year. (b)  $\delta^{18}\text{O}_{\text{gcenter}}$  profile at mid-January for each year. (c) Repartition of  $\delta^{18}\text{O}_{\text{gcenter}}$  values as a function of time  
 1138 and depth. (d) Evolution of  $\delta^{18}\text{O}_{\text{gcenter}}$  values after burial for 4 selected layers (deposited in winter 2000, and summer  
 1139 2002, 2004, 2006). Note that we do not present the evolution of snow composition in the first year after deposition  
 1140 because the thin snow layers resulting from precipitation are getting merged.  
 1141

1142



1143

1144 **Figure 9.** Test of the sensitivity of the model to the ratio of mass between grain surface compartments and total grain  
 1145 and to the interval of mixing between the two compartments (GRIP).



1146  
 1147 **Figure 10.** Test of the sensitivity of the model to the ratio of mass between surface and grain center compartments  
 1148 and to the interval of mixing between the two compartments (Dome C).